Quaternary Science Reviews 324 (2024) 108466

Contents lists available at ScienceDirect

Quaternary Science Reviews

journal homepage: www.elsevier.com/locate/quascirev

Late-Holocene ecosystem dynamics and climate sensitivity of a permafrost peatland in Northeast China

Yingfan Xia [a], Zili Yang [a], Jingjing Sun [a], Zhengyu Xia [a], Zicheng Yu [a,b,c,*]

[a] Key Laboratory of Geographical Process and Ecological Security in Changbai Mountains, Ministry of Education, School of Geographical Sciences, Northeast Normal University, Changchun, Jilin, 130024, China
[b] State Key Laboratory of Black Soils Conservation and Utilization, Northeast Institute of Geography and Agroecology, Chinese Academy of Sciences, Changchun, Jilin, 130102, China
[c] State Environmental Protection Key Laboratory of Wetland Ecology and Vegetation Restoration, Northeast Normal University, Changchun, Jilin, 130024, China

ARTICLE INFO

Handling Editor: Dr Yan Zhao

Keywords:
Permafrost peatland
Ecosystem dynamics
Fen-bog transition
Carbon accumulation
Late Holocene
Northeast China

ABSTRACT

Northern peatlands play an important role in the global carbon cycle. Here we use multi-core and multi-proxy records from a peatland near Darbin Lake in the Arxan region of Northeast China—near the southernmost limit of circum-Arctic permafrost and the northern limit of East Asian summer monsoon influence—to document peatland development and carbon accumulation histories and their responses to past climate changes during the last 2500 years. Our macrofossil results show that the peatland was characterized by a sedge-dominated fen from 500 BCE to 1450 CE, changed to a *Sphagnum*-dominated poor fen or bog with abundant shrubs between 1450 and 1960 CE, and finally became predominated by *Sphagnum* mosses after 1960 CE. The time-weighted mean apparent carbon accumulation rates from three cores ranged from 19.5 to 53.0 g C m^{-2} yr^{-1} with a mean value of 32.4 g C m^{-2} yr^{-1}, but increased rapidly to 139.2 g C m^{-2} yr^{-1} during the last several decades. During the early stage of the peatland development, three coring sites that are only 50 m apart were all in the fen phase but they had highly variable bulk densities. The fen-bog transition at these locations occurred during the Little Ice Age but at different times owing to the various influences of local hydrology, permafrost dynamics, or fire disturbance. These observations suggest that fens are highly heterogeneous, not only in peat properties but also in ecosystem dynamics. The dramatic increases in apparent carbon accumulation rates during the late stage of the bog phase after 1960 CE cannot be entirely explained by the limited decomposition of recently accumulated young peat. Instead, our analysis suggests that this was likely due to the increasing *Sphagnum* dominance and low decomposition of *Sphagnum*-derived litter, supporting the notion of the important role of vegetation changes in controlling carbon accumulation rates of peatlands. Around the 1990s CE, an increase in allogenic carbon accumulation rate—after removing the effect of age-related long-term autogenic decay of peat—coincides with a period of increased regional summer precipitation, suggesting the high sensitivity of continental ombrotrophic bog ecosystems to hydroclimate changes at decadal timescales.

1. Introduction

Peatlands are a large terrestrial carbon stock that contains ca. 600 Gt C (Yu et al., 2010) and play an important role in the global carbon cycle (Frolking and Roulet, 2007; MacDonald et al., 2006; Yu, 2011). The development and carbon accumulation of peatlands reflect the balance between the net primary productivity of peat-forming plants and the decomposition of organic matter (OM), both of which are influenced by climate change and also in turn affect the climate through carbon cycle-climate feedback. With climate warming, peatlands could change from a carbon sink to a carbon source, further amplifying climate warming (Gallego-Sala et al., 2018). The future vulnerability of large peatland carbon stocks therefore calls for a better understanding of the responses of peatland ecosystems and carbon dynamics to past climate changes.

The recent peatland data syntheses for the Holocene (Yu et al., 2009) and the last millennium (Charman et al., 2013) suggest that carbon accumulation rates of peatlands are higher during the warm periods as longer and warmer growing seasons promote plant production more than OM decomposition, providing negative feedback to climate change

* Corresponding author. School of Geographical Sciences, Northeast Normal University, Changchun, Jilin, 130024, China.
E-mail address: yuzc315@nenu.edu.cn (Z. Yu).

https://doi.org/10.1016/j.quascirev.2023.108466
Received 1 June 2023; Received in revised form 27 November 2023; Accepted 5 December 2023
0277-3791/© 2023 Elsevier Ltd. All rights reserved.

(Gallego-Sala et al., 2018; Jones and Yu, 2010; Loisel and Yu, 2013; Yu et al., 2010). Rapid warming in mid- and high-latitudes in recent decades has caused multiple changes in peatland ecosystems (Magnan et al., 2021; Sim et al., 2019) and affected the peatland carbon dynamics (MacDonald et al., 2006; Yu, 2011). For example, the recent climate-induced colonization or expansion of *Sphagnum* mosses and the substantial increases in carbon accumulation rates have been observed in peatlands worldwide (Loisel and Yu, 2013; Magnan et al., 2021; Piilo et al., 2023; Robitaille et al., 2021). Loisel and Yu (2013) developed a conceptual model to demonstrate the positive effects of recent warming on *Sphagnum* growth and peatland carbon accumulation. However, some studies have also suggested that a higher temperature will lead to accelerating microbial activity (Dorrepaal et al., 2009) and permafrost thaw particularly near the southern range limit of permafrost-affected peatlands (Hugelius et al., 2020; Jones et al., 2017). These changes could release more carbon from peatlands to the atmosphere, resulting in positive feedback to climate change.

The hydrology of peatlands affects their vegetation succession and productivity as well as aerobic/anaerobic decomposition processes, thereby affecting the peatland carbon balance (Loisel and Garneau, 2010; Zhang et al., 2018a, 2022). However, the complex ecohydrological feedback systems of peatlands varying between and within sites (Zhang et al., 2022) lead to great uncertainties in understanding the response of peatland ecosystems and carbon dynamics to climate changes (Magnan et al., 2021; Piilo et al., 2020; Sim et al., 2021; Zhang et al., 2018a). For example, the warming-induced permafrost thaw and increases in evapotranspiration rates in high-latitude peatlands may lead to both wetter and drier conditions in peatlands, respectively (Sim et al., 2021). Furthermore, short-term (decadal to centennial) climate changes can have long-term (centennial to millennium) effects on the ability of peatlands to maintain a positive carbon balance (Friedlingstein et al., 2006; Frolking et al., 2010). However, there are still few studies on the responses of peatland carbon dynamics to climate changes at decadal and centennial timescales (Yu, 2012).

Northeast China is located near the southern distribution range of northern peatlands. A number of studies have been published to understand the long- and short-term peatland carbon dynamics in this region (Xing et al., 2015; Bao et al., 2011, 2015). Based on the peatland core data synthesis, Xing et al. (2015) found that photosynthetically active radiation over the growing season determined the long-term carbon accumulation rates, but did not present a detailed discussion on the long-term peatland evolution and the recent peatland response to climate warming. Bao et al. (2015) estimated recent carbon accumulation rates in the region for the last 200 years but did not discuss the relationship between climate change and carbon accumulation. The studies by Liu et al. (2019) and Wang (2021) partly filled this knowledge gap, but the former lacked attention to the relationship between peatland ecosystem evolution and carbon dynamics, while the latter discussed the impact of climate on carbon accumulation without excluding autogenic processes. Furthermore, the southern limit of the permafrost distribution area in Northeast China has moved northward in recent decades as a result of active layer deepening and permafrost thaw (Jin et al., 2000; Zhang et al., 2021), which would affect the carbon balance of these permafrost-affected peatlands. However, previous studies from the region have seldom addressed the carbon accumulation histories and dynamics of these permafrost-affected peatlands.

The Darbin Lake peatland in the Greater Khingan Mountains of Northeast China is located at the southernmost limit of the circum-Arctic permafrost region (Brown et al., 2002; Jin et al., 2016) and the northern limit of the East Asian summer monsoon region (Chen et al., 2008). Here we use multi-core and multi-proxy records (1) to reconstruct the development history of the peatland, (2) to document the temporal pattern of peatland carbon accumulation, and (3) to discuss the response of peatland development and carbon accumulation to climate change. To our knowledge, this is the first study that documents ecosystem and carbon accumulation histories of permafrost-affected peatlands in Northeast China, which will deepen our understanding of how northern peatlands respond to future climate changes.

2. Study region and sites

Darbin Lake (also known as Songye Lake) is a volcanic dammed lake formed by the lava flow of the Arxan volcanic eruption during the Quaternary period. It is located at the northeast slope of Motianling, a peak on the western side of the middle section of the Greater Khingan Mountains (Fig. 1a; Zhang et al., 2014). The Halaha River enters from the southeast of Darbin Lake and flows out through the northwest end of the Lake. The study region has a temperate continental climate with a mean annual temperature of −2.7 °C and a mean annual precipitation of 440 mm (Arxan meteorological station, 47.17°N, 119.93°E, elevation ~997 m a.s.l., about 60 km from Darbin Lake).

Darbin Lake peatland (47.40340°N, 120.66131°E, elevation ~1300 m a.s.l.) is about 370 m west of Darbin Lake. The peatland area is approximately 0.6 km^2 in size and is relatively flat with some hummocky microtopography (Fig. 1d). The peatland is dominated by mosses including *Sphagnum rubellum, S. squarrosum*, *S. magellanicum*, *S. acutifolium*, *S. girgensohnii*, *Polytrichum strictum*, and *Drepanocladus aduncus*, accompanied by shrubs including *Betula ovalifolia, Vaccinium utisidaea, Ledum palustre* var. *angustum*, *Carex* spp., and *Calamagrostis angustifolia*. *Larix gmelini* is abundant on the hillsides around the peatland (Fig. 1d). The region is within the isolated permafrost zone (Brown et al., 2002; Jin et al., 2016), and we encountered permafrost during peat coring in August 2018.

3. Materials and methods

3.1. Sample collections

In August 2018, three peat cores were collected from three well-developed hummocks at Darbin Lake peatland that are ~50 m apart for the following analysis to avoid the bias of single-core analysis, labeled as DL18-C1, DL18-C2, and DL18-C3 (Fig. 1c and Table 1). The upper monoliths of the cores were collected by using a stainless serrated knife to avoid compression, and the corresponding deeper parts were collected with a 7 cm × 7 cm box corer (< 20 cm apart from the monolith). These sections were combined to generate three contiguous cores (Table 1). Peat cores were wrapped with plastic film, placed in the polyethylene pipes in the field, transported back to the laboratory, and stored in frozen conditions. The cores were cut into 1 cm-thick slices using a band saw and sealed in plastic bags. Subsamples were stored in frozen conditions before further analyses.

3.2. Radiocarbon dating

The chronology of the three cores was determined using accelerator mass spectrometry (AMS) radiocarbon (^{14}C) dating. To obtain credible ages, we chose the aboveground parts of plant remains as dating materials. All the AMS ^{14}C dating samples were pretreated by the standard acid-alkali-acid protocol, and then freeze-dried in an ultra-low temperature vacuum. The graphite targets were prepared at Northeast Normal University or National Taiwan University AMS (NTUAMS) Lab and then were analyzed in the NTUAMS Lab for ^{14}C dating. Pre- and post-bomb ^{14}C dates were calibrated to calendar ages with IntCal 20 (Reimer et al., 2020) and Bomb 21 NH1 datasets (Hua et al., 2022) on OxCal v4.4 program (https://c14.arch.ox.ac.uk/oxcal/OxCal.html), respectively, for an overview as listed in Table 2.

The age-depth models of the three peat cores were generated using the Bacon program (Blaauw and Christen, 2011). For prior parameter information, we set 3 cm as the thickness of each section, which was used to make the age-depth curve as smooth as possible without unexplained turning points in non-dating levels. The prior for accumulation rates was set to the default value *acc. shape* = 1.5 for three cores, and *acc.*

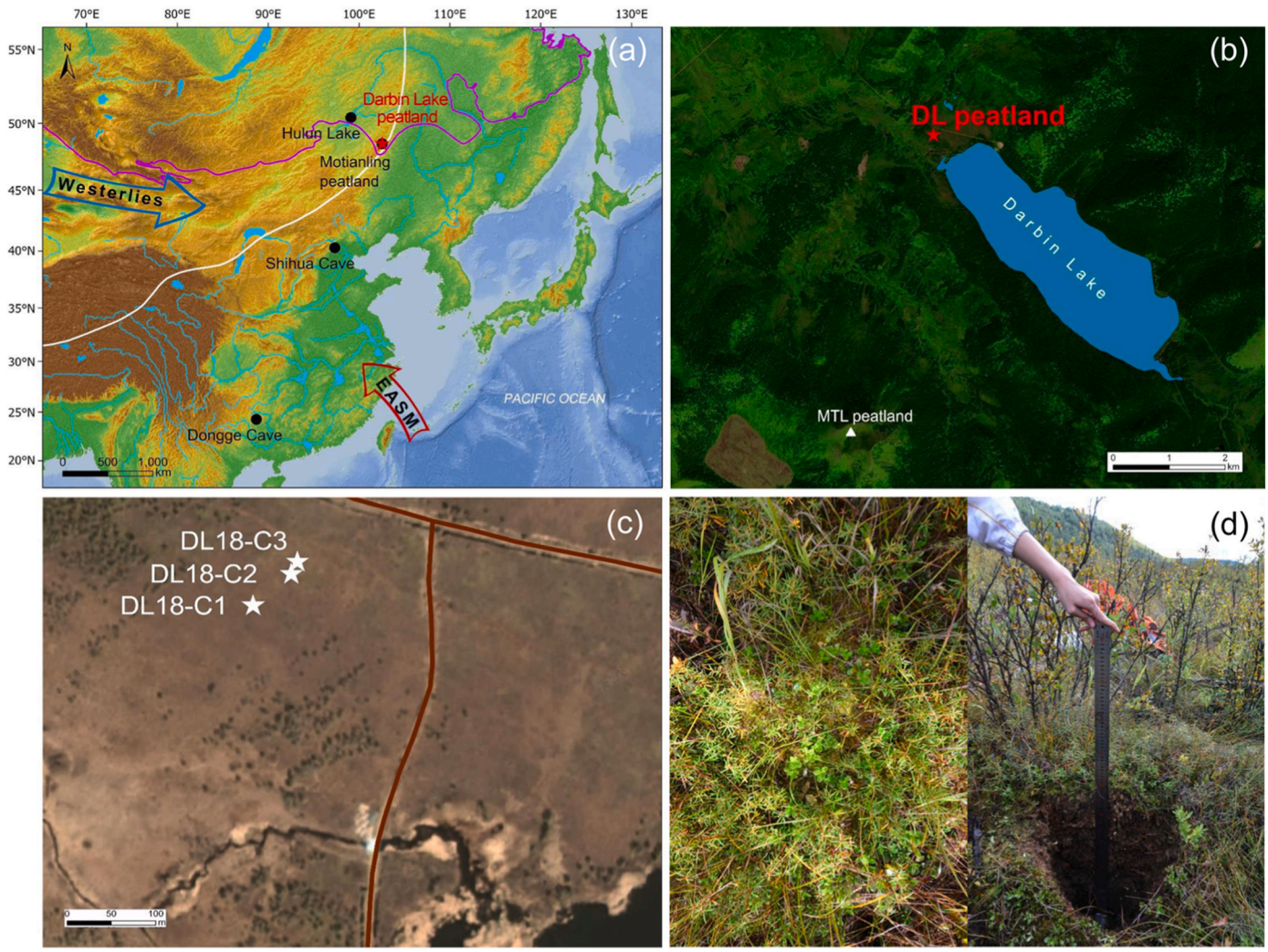

Fig. 1. Settings of the study region and site in Northeast China. (a) The locations of Darbin Lake peatland (red star) and other paleoclimate records discussed in this paper (black dots). EASM: East Asian summer monsoon. The limit of the modern Asian summer monsoon region (white line) is from Chen et al. (2008). The southernmost limit of the circum-Arctic permafrost region (purple line) is from Brown et al. (2002). (b) Landscape characteristics of the Darbin Lake peatland. The white triangle is Motianling peatland (Bao et al., 2012). (c) The locations of peatland cores DL18-C1, DL18-C2, and DL18-C3. The brown lines are roads. (d) Photos of vegetation near the coring sites.

Table 1
Information of peat cores from Darbin Lake peatland.

Core ID	Latitude (°N)	Longitude (°E)	Elevation (m a.s.l.)	Core length (cm)	Water table depth (cm)
DL18-C1	47.40322	120.66097	1296	66	NA
DL18-C2	47.40345	120.66136	1298	71	26
DL18-C3	47.40353	120.66142	1300	92	40

mean = 50 for DL18-C1 and DL18-C2 suggested by Bacon (due to initial estimates of accumulation rates that differ much from the default prior *acc. mean*) and default *acc. mean* = 20 for DL18-C3. As for the memory prior, we kept the default values (*mem.strength* = 4 and *mem. mean* = 0.7).

3.3. Peat property analysis

Subsamples of 1 cm^3 in volume were extracted at 1-cm intervals from three cores for loss-on-ignition (LOI) analysis (Chambers et al., 2011). We first dried the subsamples at 105 °C in an oven for 12 h to estimate water content (WC; %). Dry bulk density (DBD; g cm^{-3}) was obtained by dividing dry weight by fresh subsample volume. Then we combusted the subsamples at 550 °C in a muffle furnace for 4 h to make sure that all organic matter was burned to estimate organic matter content (OM; %). Ash content (AC; %) was equivalent to 100–OM (%). Organic matter bulk density (OMBD; g cm^{-3}) was obtained by multiplying DBD and OM. All samples were processed with the same ignition temperature, burning time, and sample size to achieve comparability between three cores (Heiri et al., 2001).

3.4. Grain size analysis

The grain sizes of core DL18-C1 were analyzed to constrain the source of the mineral materials at Darbin Lake peatland. We added 5 mL of 10% HCl to the peat ash subsamples obtained after burning at 550 °C

Table 2
Radiocarbon dates of peat cores from Darbin Lake peatland.

Lab Code[a]	Depth (cm)	Material Dated	pMC ± Error (%)[b]	Radiocarbon Date ± Error (^{14}C yr BP[c])	Calibrated Age 2σ Range (cal yr BP)	Calibrated Median Age (cal yr BP; cal. yr in CE in brackets)[e]
Core: DL18-C1						
NTUAMS-6721s	10–11	*Sphagnum* leaves	112.06 ± 1.25	−915 ± 90	−7 to −8 −40 to −50[d]	−42 (1992)
NTUAMS-6722s	20–21	*Sphagnum* leaves/stems	110.58 ± 2.18	−810 ± 160	−7 to −8[d] −50 to −56	−9 (1959)
NTUAMS-6723[f]	27–28	Charcoal	80.75 ± 0.83	1715 ± 85	1819–1405	369 (1581)
NTUAMS-6724	44–45	Herbaceous leaves/stems and ligneous leaves	86.81 ± 0.91	1135 ± 85	1278–910	1124 (826)
NTUAMS-6725s	62–63	*Sphagnum* leaves and herbaceous leaves/stems	74.06 ± 1.46	2410 ± 160	2847–2011	2281 (−331)
Core: DL18-C2						
NTUAMS-6726	7–8	*Sphagnum* leaves/stems	102.07 ± 1.09	−165 ± 85	253–227 137–115 70–39 −3 to −6 −57 to −68[d]	−49 (1999)
NTUAMS-6727	13–14	*Sphagnum* leaves/stems	104.47 ± 0.99	−350 ± 75	−5 to −7[d] −55 to −65	−5 (1955)
NENUR −10592	24–25	*Sphagnum* and herbaceous leaves/stems	100.04 ± 0.76	−5 ± 60	267–14	217 (1733)
NTUAMS-6728	32–33	Herbaceous leaves/stems and ligneous leaves	98.33 ± 1.12	135 ± 90	421–78	413 (1537)
NENUR −10593	44–45	Herbaceous leaves/stems and ligneous leaves	84.90 ± 0.66	1315 ± 60	1342–1073	1150 (800)
NENUR −10594	59–60	Herbaceous leaves/stems and ligneous leaves	81.61 ± 0.65	1630 ± 65	1696–1375	1572 (378)
NENUR −10595	69–70	Herbaceous leaves/stems and ligneous leaves	77.43 ± 0.64	2055 ± 65	2296–1829	2011 (−61)
Core: DL18-C3						
NENUR −10528	15–16	*Sphagnum* leaves/stems	104.54 ± 0.84	−355 ± 65	−5 to −7 −55 to −64[d]	−55 (2005)
NENUR −10529	23–24	*Sphagnum* leaves/stems	110.61 ± 0.82	−810 ± 60	−7 to −8 −45 to −50[d]	−46 (1996)
NENUR −10530	31–32	*Sphagnum* leaves/stems	117.98 ± 0.84	−1330 ± 60	−8 to −9 −35 to −40[d]	−34 (1984)
NENUR −10531	39–40	*Sphagnum* leaves	104.75 ± 0.78	−375 ± 60	−6 to −7[d] −55 to −63	−6 (1956)
NENUR −10532	45–46	*Sphagnum* leaves	99.72 ± 0.77	25 ± 60	270–10	35 (1915)
NENUR −10533[f]	55–56	*Sphagnum* leaves	122.80 ± 0.88	−1650 ± 60	−9 to −12 −32 to −35[d]	103 (1847)
NENUR −10534	63–64	*Sphagnum* leaves	98.86 ± 0.74	90 ± 60	278–6	233 (1717)
NENUR −10535	71–72	Herbaceous leaves/stems	98.96 ± 0.76	85 ± 60	277–6	406 (1544)
NENUR −10536	79–80	Herbaceous leaves/stems and ligneous leaves	87.84 ± 0.64	1040 ± 60	1068–790	968 (982)
NENUR −10537	84–85	Herbaceous leaves/stems and ligneous leaves	83.19 ± 0.64	1480 ± 60	1516–1292	1320 (630)
NENUR −10538	90–91	*Sphagnum* leaves	81.52 ± 0.69	1640 ± 70	1700–1378	1456 (494)

[a] Samples with the lab code prefix "NENUR" were prepared for graphite targets at Northeast Normal University and dated at National Taiwan University AMS (NTUAMS) Lab. Samples with the lab code prefix "NTUAMS" were prepared and dated at NTUAMS Lab. Samples with the lab code tail of "s" mean the graphite targets were prepared using a small volume of gas.
[b] pMC: percentage of modern radiocarbon.
[c] BP: before present (present is 1950 CE).
[d] These post-bomb^{14}C dates have one calibrated age interval on each side of the 1963 CE post-bomb^{14}C peak. Considering the stratigraphic position and peat accumulation rates, we used the most likely ages (marked by[d]) as the calibrated calendar year to input the Bacon age modeling. NTUAMS-6726 has some other older ages after calibration due to the large error of post-bomb^{14}C dates, resulting in more than two calibrated age intervals that were not considered.
[e] Calibrated median ages were obtained by age-depth modeling using the Bacon program.
[f] These dates are outliers, which were rejected by the Bacon program.

and then added 5 mL 0.05 mol/L $(NaPO_3)_6$ to facilitate dispersion. We used a MICROTRAC S3500 particle analyzer to quantify the component of clay (< 4 μm), silt (4–63 μm), and sand (63–2000 μm) for each subsample, and then calculated the median grain size.

3.5. Plant macrofossil and decomposition degree analysis

The compositions of plant macrofossils for three cores were analyzed mostly at 4-cm intervals but at 1 or 2-cm intervals for selected periods if helpful. Subsamples of 1 cm^3 in volume were boiled with 2% NaOH for 12 h to remove humic and fulvic acids. Then, subsamples were rinsed

with distilled water using a 125-μm sieve. We quantified the abundance of fine debris fraction (unidentifiable organic matter, UOM) to estimate the degree of decomposition. We used the Quadrat and Leaf Count Macrofossil Analysis (QLCMA) method (Mauquoy et al., 2010) to estimate the percentage of plant debris (including *Sphagnum* mosses, other mosses, herbaceous fragments, ligneous fragments, and charcoal) from at least 20 views under a stereomicroscope.

3.6. Apparent carbon accumulation rate

The apparent carbon accumulation rate (aCAR; g C m^{-2} yr^{-1}) for each 1-cm peat subsample from each core was calculated by multiplying three metrics: (1) the peat accumulation rate (cm yr^{-1}) based on the mean ages derived from the Bacon age-depth models, (2) the dry bulk density, and (3) the carbon content of organic matter that we assumed as a constant of 50% consistently in this paper based on published data of this region (Bao et al., 2011; Xing et al., 2015).

3.7. Modeling peatland carbon dynamics

Following the previous study by Loisel and Yu (2013), we used three modeling approaches, i.e., the exponential decay model (EDM; Clymo, 1984), the carbon flux reconstruction model (CFM; Yu, 2011), and the peat decomposition model (PDM; Frolking et al., 2001) to compare recent carbon accumulation with that of the past when taking into account that surface peat is incompletely decomposed (Bunsen and Loisel, 2020; Loisel and Yu, 2013; Wang et al., 2015; Zhang et al., 2018a). The general guidelines and detailed formula and explanation of terms for the three models are available in Appendix A. For modeling inputs, we identified the acrotelm/catotelm boundary based on the water table depth measured in the field and the changes in dry bulk density and water content (Clymo, 1984). To obtain p and a in EDM, we input the time (x) and cumulative peat mass (y) data in the Origin software (OriginLab Corporation, USA), construct a custom function in the form of $y = b/a\text{-}(b/a)*(\exp(-a*x))$ (a is α; b is p), select that function in the *Nonlinear Curve Fit* module, enter the prior estimated values of p and a in the *Value* column under the *Parameters* module, and finally perform the nonlinear fitting.

To explore the effect of allogenic factors (such as climate) on carbon accumulation rates in recent decades, following Zhang et al. (2018a) we calculated the modeled CAR (i.e., autogenic CAR, affected by the effect of age-related long-term decay on peat) based on the derived p and a from the EDM. Then, the differences between aCAR and autogenic CAR were considered to be the allogenic CAR (expressed as CAR z scores) driven by allogenic factors (Zhang et al., 2018a, 2020).

4. Results and interpretations

4.1. Chronology and peat accumulation rate

The ^{14}C dates and calibrated ages of 23 samples from three cores are shown in Table 2. We note that our ^{14}C chronology is in quite high-resolution for a late-Holocene study, but the error bar of ^{14}C dates is larger than usual. The age-depth models (Fig. 2) show that the oldest (not basal) ages of core DL18-C1, DL18-C2, and DL18-C3 are ca. 500 BCE, 100 BCE, and 450 CE, respectively. The mean peat accumulation rates and standard deviations for 1-cm slices of three cores are 0.117 ± 0.155 cm yr^{-1}, 0.095 ± 0.164 cm yr^{-1}, and 0.374 ± 0.407 cm yr^{-1}, respectively (Table 3). The relatively large standard deviations show significant fluctuations during the past peat accumulation history. Cores DL18-C2 and DL18-C3 showed slightly higher accumulation rates in the early stage, followed by slower accumulation rates. All three cores accumulated peat rapidly after ca. 1960 C E. It should be noted that DL18-C1 has a less robust age-depth model than the other two cores due to fewer dating points (Fig. 2).

4.2. Peat properties

The peat properties of three cores at Darbin Lake peatland are shown in Fig. 3 and Table 3. The organic matter (OM) and water content (WC) show overall increasing trends towards the core top, while dry bulk density (DBD), ash content (AC), and organic matter bulk density (OMBD) show the opposite trends. The OM values (74.9 ± 14.7%; mean ± S.D.) for three cores are close the previously reported values for peatlands in the Greater Khingan Mountains (63.3 ± 5.9%; Xing et al., 2015) and northern peatlands (90.7 ± 13.0%; Loisel et al., 2014). The DBD values (0.246 ± 0.179 g cm^{-3}) are higher than that in northern peatlands (0.118 ± 0.069 g cm^{-3}; Loisel et al., 2014), but are similar to the value in the Greater Khingan Mountains (0.217 ± 0.090 g cm^{-3}) reported by Xing et al. (2015). Compared to cores DL18-C1 and DL18-C2, the mean values and standard deviations of DBD and OMBD of core DL18-C3 are the largest. There is a negative correlation between AC and WC ($r = -0.85$, $p < 0.001$) (Fig. 4a), and a positive correlation between AC and OMBD ($r = 0.63$, $p < 0.001$) (Fig. 4b).

4.3. Grain size

The peat ash grain size component of core DL18-C1 is dominated (> 95%) by the small size fraction of < 100 μm. Silt content (81.2–94.0%) is higher than clay content (2.1–11.1%) and sand content (1.8–16.5%; Fig. 5a). The median grain size values range from 14.8 to 32.4 μm, and the mean value is 19.7 μm (Fig. 5b). The grain-size frequency distributions of peat ash show single kurtosis (Fig. 5c), which may reflect that the mineral inputs in this region are from a single source (Bao et al., 2010).

4.4. Past vegetation changes and decomposition

The macrofossil results reflect the vegetation changes and the stages of peatland development histories at Darbin Lake peatland (Fig. 3). Core DL18-C1 was predominated by herbaceous plants (mainly sedge) with some ligneous remains from ca. 500 BCE to 1650 CE, and *Sphagnum* mosses occurred briefly between ca. 500 BCE and 250 CE. At ca. 1650 CE, while the herbaceous decreased rapidly, the ligneous increased. *Sphagnum* mosses became predominant after ca. 1960 CE but were replaced by other dry-adapted mosses (such as *Polytrichum strictum*) at ca. 2000 CE. Core DL18-C2 was mainly predominated by herbaceous plants between ca. 100 BCE and 1960 CE, but the ligneous increased during the period ca. 1500–1800 CE, and the charcoal peak appeared ca. 1650 CE. From ca. 1960 CE, *Sphagnum* mosses recolonized with some other mosses and ligneous plants. Core DL18-C3 was mainly predominated by herbaceous plants from ca. 450 CE to 1550 CE, but ligneous increased from ca. 850 to 1450 CE. There are two charcoal peaks between ca. 1050 and 1450 CE. *Sphagnum* mosses appeared at ca. 1450 CE, developed rapidly after ca. 1550 CE, and have been predominant until the present, accompanied by a few ligneous and herbaceous plants. The unidentifiable organic matter (UOM) of three cores generally shows decreasing trends, with some fluctuations, towards the top with *Sphagnum* mosses becoming predominated. Ash content has positive correlations with UOM ($r = 0.66$, $p < 0.001$), ligneous percentage ($r = 0.29$, $p < 0.01$), and charcoal percentage ($r = 0.48$, $p < 0.001$) (Fig. 4c–e).

4.5. Apparent carbon accumulation rate variability

The time-weighted mean aCAR for three cores are 19.5 g C m^{-2} yr^{-1}, 24.7 g C m^{-2} yr^{-1}, and 53.0 g C m^{-2} yr^{-1}, respectively, and the mean value is 32.4 g C m^{-2} yr^{-1} (Fig. 3 and Table 3). This value is surprisingly the same as the reported mean value of peatland aCAR (32.4 g C m^{-2} yr^{-1}; Xing, 2017) during the past 2000 years in the previous peatland data synthesis in Northeast China. The aCAR of three cores increased rapidly after ca. 1960 CE, to a time-weighted mean value of 139.2 g C

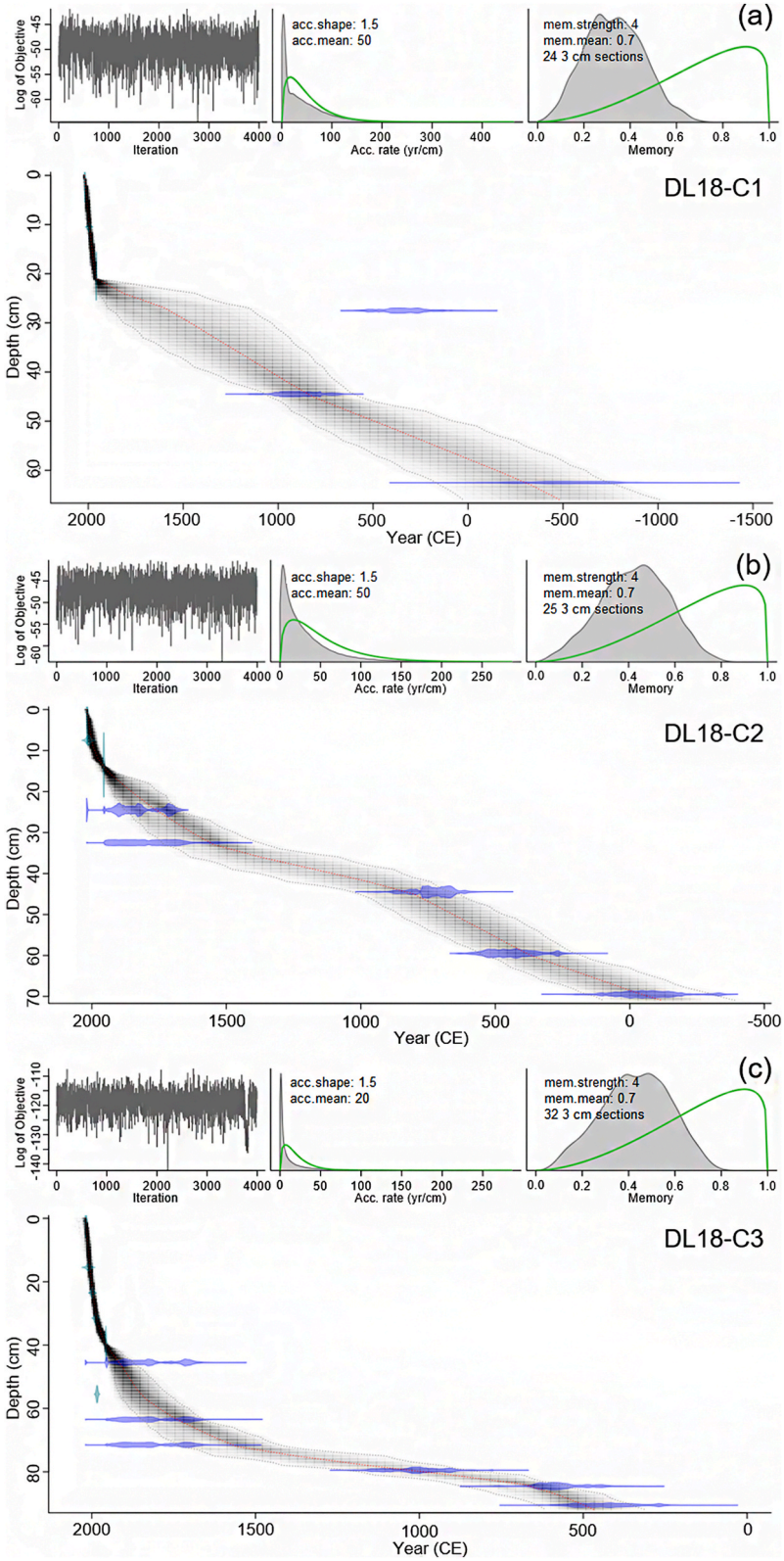

Fig. 2. Bacon age-depth models of core (a) DL18-C1, (b) DL18-C2, and (c) DL18-C3. The cyan symbols show the post-bomb ages that were determined on the basis of stratigraphic position and were set as "calendar ages" for inputs to the Bacon program, and the blue symbols are pre-bomb ages that we set as uncalibrated ages for the Bacon program.

Table 3
Mean values of peat properties with standard deviation (±SD) from Darbin Lake peatland. OM: organic matter; DBD: dry bulk density; AC: ash content; OMBD: organic matter bulk density; WC: water content; PAR: peat accumulation rate; aCAR: apparent carbon accumulation rate.

Core	OM (%)		DBD (g cm^{-3})		AC (%)		OMBD (g cm^{-3})	
	Mean ± SD	Range	Mean ± SD	Range	Mean ± SD	Range	Mean ± SD	Range
DL18-C1	72.3 ± 11.3	53.9–92.8	0.242 ± 0.115	0.051–0.455	27.7 ± 11.3	7.2–46.1	0.165 ± 0.071	0.043–0.266
DL18-C2	69.2 ± 16.8	39.6–99.4	0.235 ± 0.161	0.019–0.578	30.8 ± 16.8	0.6–60.4	0.140 ± 0.081	0.017–0.290
DL18-C3	81.3 ± 13.0	53.7–98.4	0.259 ± 0.228	0.046–0.851	18.7 ± 13.0	1.6–46.3	0.183 ± 0.131	0.041–0.472
All cores	74.9 ± 14.7	39.6–99.4	0.246 ± 0.179	0.019–0.851	25.1 ± 14.7	0.6–60.4	0.164 ± 0.103	0.017–0.472
Core	WC (%)		PAR (cm yr^{-1})		aCAR (g C m^{-2} yr^{-1})		Time-weighted mean aCAR (g C m^{-2} yr^{-1})	
	Mean ± SD	Range	Mean ± SD	Range	Mean ± SD	Range		
DL18-C1	73.0 ± 6.3	60.0–87.4	0.117 ± 0.155	0.008–0.500	49.2 ± 53.6	10.4–216.5	19.5	
DL18-C2	76.0 ± 9.5	61.2–93.1	0.095 ± 0.164	0.013–1.000	32.4 ± 31.9	5.4–216.0	24.7	
DL18-C3	84.2 ± 8.3	65.9–92.6	0.374 ± 0.407	0.011–1.100	160.8 ± 130.3	23.2–535.5	53.0	
All cores	78.4 ± 9.4	60.0–93.1	0.212 ± 0.313	0.008–1.100	88.2 ± 106.6	5.4–535.5	32.4	

m^{-2} yr^{-1}.

4.6. Modeled peat decay and carbon dynamics

Considering that cores DL18-C2 and DL18-C3 have more than four dating horizons in the acrotelm and the catotelm (the surface of the peat core has a coring "age" of 2018 CE), we run the exponential decay model on these two cores (Clymo, 1984). The results show that core DL18-C2 presents a concave curve in the acrotelm, where the peat addition rate (p) and peat decay coefficient (α) are 110 g m^{-2} yr^{-1} and 0.0075 yr^{-1}, respectively (Fig. 6a), and presents a convex curve in the catotelm in contrast with the standard bog growth model (i.e., concave curve). Core DL18-C3 shows concave curves in both the acrotelm and the catotelm (Fig. 6b–d). The peat addition rates in the recent decades (after 1960 CE; the top of the acrotelm), the acrotelm, and the catotelm are 795 g m^{-2} yr^{-1}, 726 g m^{-2} yr^{-1}, and 244 g m^{-2} yr^{-1}, respectively. As for peat decay coefficients, the values are 0.0114 yr^{-1}, 0.0095 yr^{-1}, and 0.0008 yr^{-1}, respectively. Combining cores DL18-C2 and DL18-C3, the mean peat addition rate and peat decay coefficients in the acrotelm at Darbin Lake peatland are 418 g m^{-2} yr^{-1} and 0.0085 yr^{-1}, quite close to other reported values from the Greater Khingan Mountains (356 g m^{-2} yr^{-1} and 0.0056 yr^{-1} in Liu et al. (2019); 389 g m^{-2} yr^{-1} and 0.0068 yr^{-1} in Wang (2021)).

The carbon flux reconstruction model of core DL18-C3 yielded net carbon uptake (NCU) values in the catotelm ranging from 30.8 to 188.6 g C m^{-2} yr^{-1}, with the mean value of 69.2 g C m^{-2} yr^{-1} (Fig. 7a). These estimates represent the peat carbon flux that entered the catotelm over the past 1600 years. The peat decomposition model of core DL18-C3 simulated peat mass loss in the acrotelm for ~300 years (Fig. 7b). Remaining peat masses are 462 g OM m^{-2} (or 231 g C m^{-2}) after 60 years and 189 g OM m^{-2} (or 94.5 g C m^{-2}) after 300 years, if the initial peat mass produced in a year is 726 g OM m^{-2} and the initial decay rate is 0.0095 yr^{-1}. These values correspond to the amount of peat that would be transferred from the acrotelm into the catotelm over time and allow us to link short- and long-term processes of peat carbon accumulation. After 60-year (for discussing carbon dynamics in recent decades) and 300-year (when the peat decomposes in the acrotelm for the longest time) acrotelm decomposition, the remaining peat carbon would still be 3.3 and 1.4 times of the mean modeled catotelm NCU, suggesting an increase in the peatland carbon sink capacity in recent centuries.

The CAR z scores for core DL-C3, which was predominated by *Sphagnum* mosses after ca. 1960 CE and has a robust age control, have undergone several major shifts since 1960 CE (Fig. 8). CAR z scores are higher during the period 1987–2004 CE and lower during the period 1960–1987 CE and 2004–2018 CE. The variations of CAR z scores seem to coincide with the summer precipitation or summer moisture index (P/E_q, where P is precipitation and E_q is potential evapotranspiration calculated from temperature; Ma and Fu, 2001), but not consistently with the summer temperature.

5. Discussion

5.1. Peatland development and carbon accumulation history

Before discussing the different stages of peatland development and carbon accumulation, we first suggest that mineral particles (i.e., peat ash) at Darbin Lake peatland were mainly transported to the site by aeolian process and are useful indicators of regional moisture conditions supported by other proxy data and published paleoclimate records in the region. The reasons are as follows: (1) Darbin Lake peatland is located in the transition zone between the semi-arid and semi-humid regions of Northeast China where dust activities are frequent. A previous study has confirmed that the Motianling peatland, which is less than 4 km from Darbin Lake peatland, is affected by the long-term atmospheric dust deposition from northern China and Mongolia based on geochemical proxies (Bao et al., 2012). (2) The northwest outlet of Darbin Lake is located in a wide and shallow river valley (Fig. 1). We did not observe any field evidence to support the influence of river water flow on the peatland. (3) Peat ash grain size data show that the mineral particles at Darbin Lake peatland were mainly silt with a mean median grain size of 19.7 μm, which indicates an aeolian genesis, and the input source was single (Fig. 5; Li et al., 2017).

The ash content (AC) in peat is often higher when the regional climate is dry—the upland vegetation cover is sparse—the transport of dust particles to the site by the westerlies is enhanced. From the physical peat property and macrofossil data, we also found that AC has positive correlations with organic matter bulk density and unidentifiable organic matter (UOM), which both indicate the degree of decomposition in peat that tends to be higher under drier conditions (Fig. 4b and c). Meanwhile, AC has positive correlations with the percentages of ligneous macrofossils and charcoals that represent relatively drier habitats at the peatland site (Fig. 4d and e). Combined with other regional paleoclimate records, we will discuss the peatland development and carbon accumulation history at Darbin Lake peatland based on the peatland development processes to understand their responses to past climate changes during the past 2500 years (Fig. 9).

Stage I (ca. 500 BCE–1450 CE): Darbin Lake peatland was a sedge-dominated fen at this stage. Between ca. 500 BCE and 200 CE, the low AC values indicate a wet climate that inhibited the dust particles inputs to core DL18-C1. The pollen-based temperature and precipitation records from Hulun Lake also suggest warm and wet conditions during this period (Wen et al., 2010, Fig. 9n and p). *Sphagnum* mosses were present in core DL18-C1, but were gradually replaced by herbaceous plants, which has been observed in other northern peatlands as well (Piilo et al., 2020; Ryberg et al., 2022; Yang et al., 2023). During the period ca. 850–1450 CE, the ligneous plant remains in core DL18-C3 increased, likely indicating the lowering water table and drying conditions (Sun et al., 2019). In addition to the decreasing precipitation recorded in Hulun Lake (Wen et al., 2010), the trends towards lower *Sphagnum* δ^{13}C

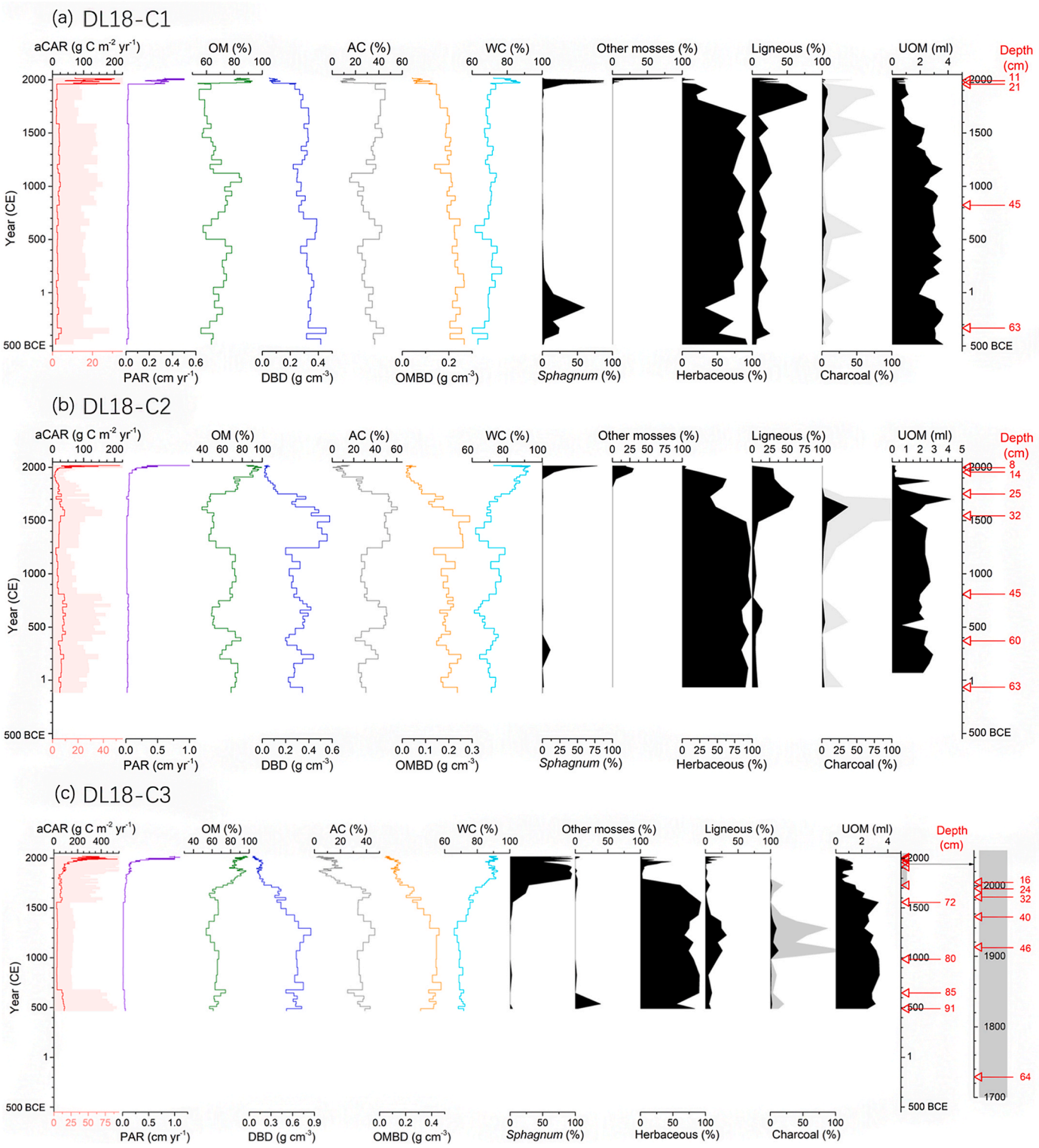

Fig. 3. Summary of peat properties and macrofossil assemblages of core (a) DL18-C1, (b) DL18-C2, (c) DL18-C3, plotted against the calendar year. The light red shadings of aCAR are for showing the smaller-magnitude variations based on the bottom red *x*-axis. The light grey shadings of the charcoal percentage indicate the results in × 10 exaggeration. The red triangles and numbers on the right indicate the horizons and depths with AMS ^{14}C dating, respectively; and the far-right shaded column in (c) shows the detail after about 1700 CE. aCAR: apparent carbon accumulation rate; PAR: peat accumulation rate; OM: organic matter; DBD: dry bulk density; AC: ash content; OMBD: organic matter bulk density; WC: water content; UOM: unidentifiable organic matter.

values (Lin et al., 2004, Fig. 9q) at Motianling peatland (the record recently verified by the more detailed measurements of *Sphagnum* stem δ^{13}C by Wang (2021); Fig. 9q) also support the dry climate during this period. The dry climate not only provided a flammable condition but also promoted woody plants' growth and provided fuels for fire occurrences (Archibald et al., 2009; Wang et al., 2013). These together resulted in increasing fire events as documented by the higher percentages of charcoal in core DL18-C3 during ca. 1050–1450 CE. The

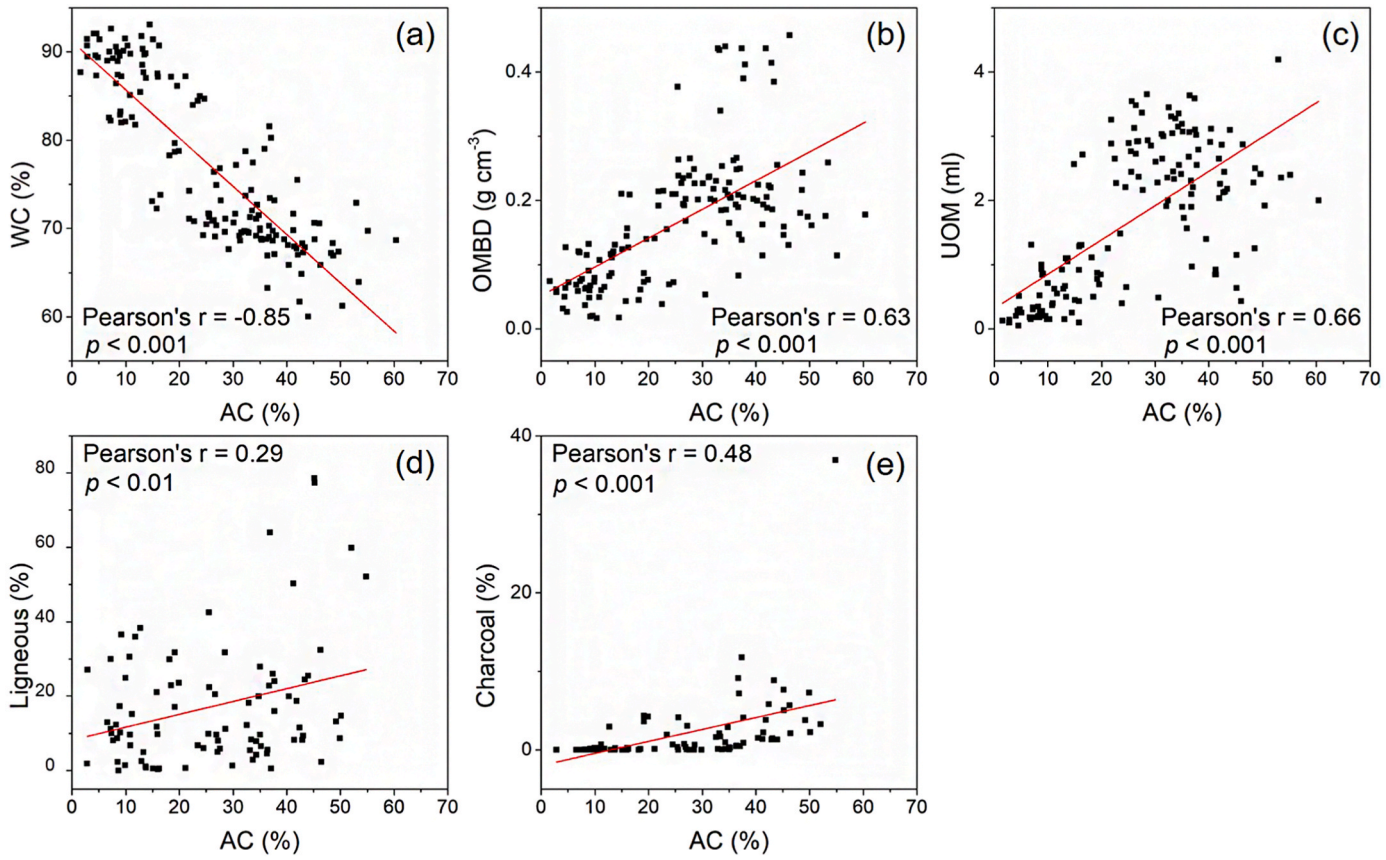

Fig. 4. The scatter plots show the relationships of ash content (AC) with (a) water content (WC), (b) organic matter bulk density (OMBD), (c) unidentifiable organic matter (UOM), (d) ligneous percentage, and (e) charcoal percentage. Red lines are regression lines.

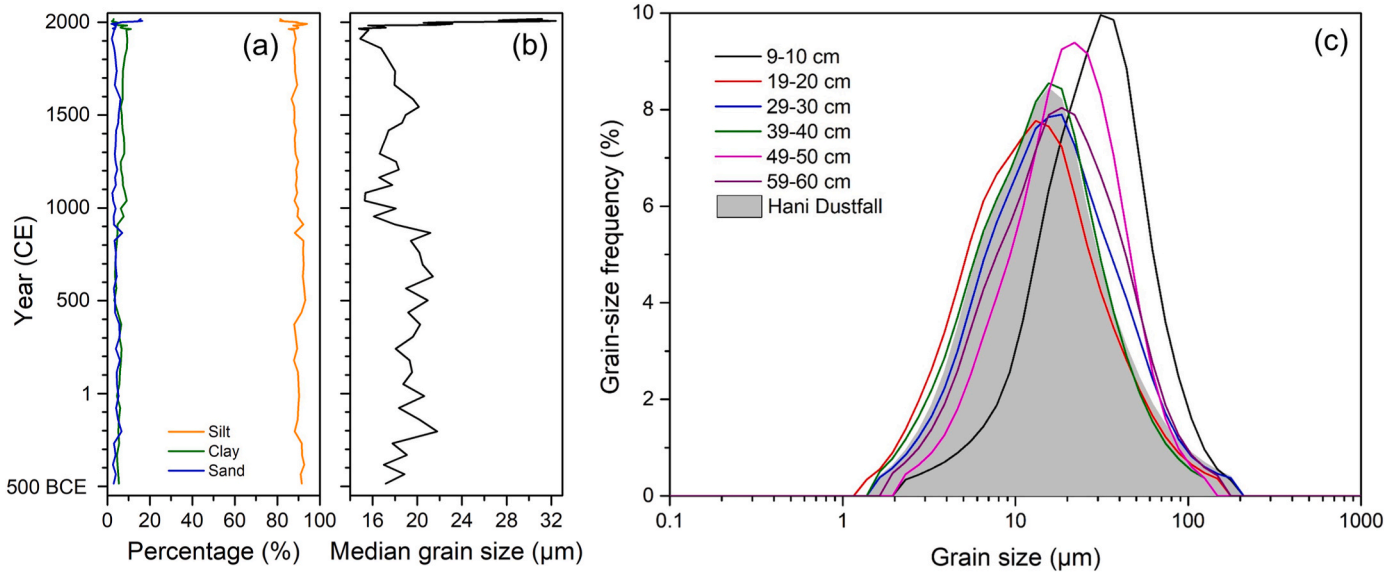

Fig. 5. The peat ash grain size results of core DL18-C1, including (a) the percentage of silt, clay, and sand, (b) the median grain size, and (c) the grain-size frequency distribution curves for selective depths.

mean value of aCAR during Stage I was 26.8 g C m^{-2} yr^{-1}, and showed little fluctuation. Overall, the peatland remained in the stable sedge-dominated fen at this stage with stable carbon accumulation rates under climate drying, which may reflect the ability of fens to maintain stability through self-regulation feedback until they reach the bifurcation (or tipping point) of fen-bog transition (FBT; Loisel and Bunsen, 2020). However, due to the lack of local hydrological records, such as testate amoebae-based water table reconstructions, we are unable to further elaborate on how the regulatory mechanism affected peatland development and carbon accumulation processes.

Stage II (ca. 1450–1960 CE): At this stage, the herbaceous plants decreased, but *Sphagnum* mosses and woody plants increased, indicating

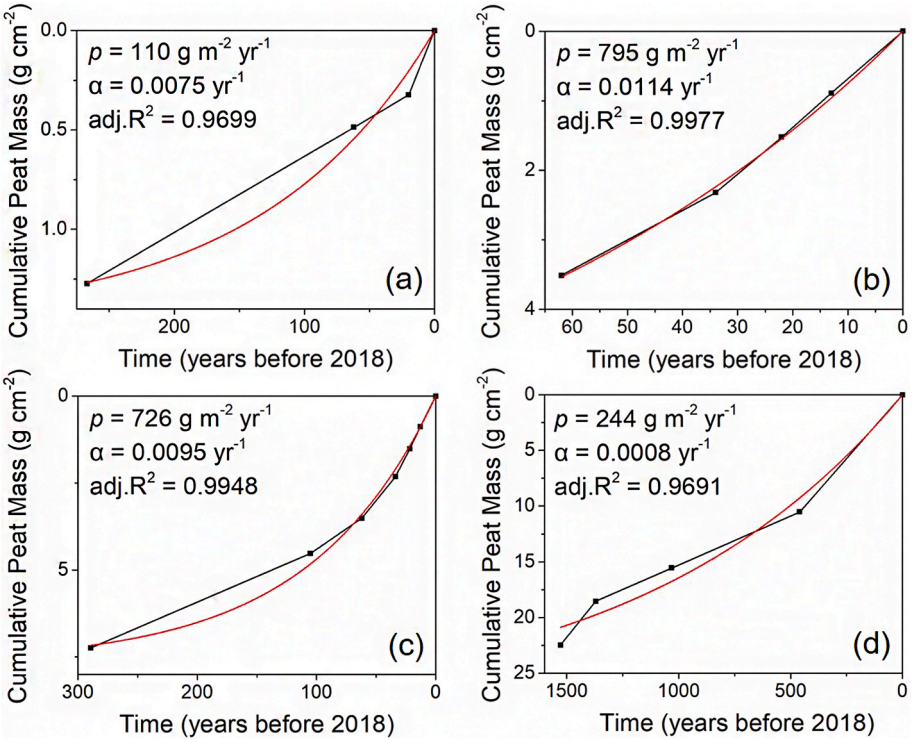

Fig. 6. Exponential decay modeling (EDM) results of core DL18-C2 in (a) the acrotelm, and core DL18-C3 in (b) the recent decades (after 1960 CE), (c) the acrotelm, and (d) the catotelm. Black squares are the calibrated ages and red lines are the results of the fitted model.

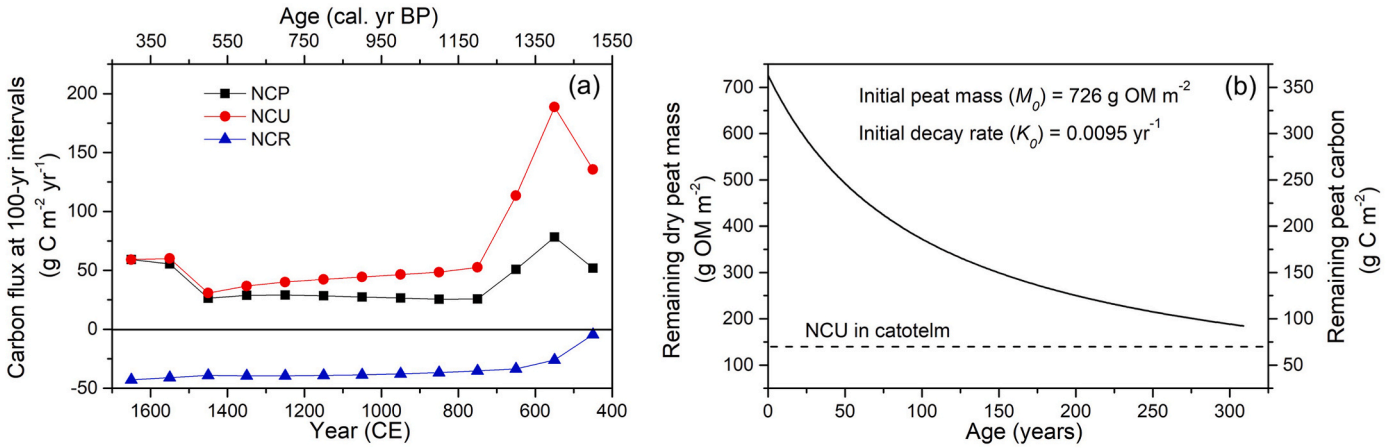

Fig. 7. (a) The peat carbon flux modeling (CFM) results from the catotelm of core DL18-C3. The net carbon pool (NCP) represents the current peat carbon stock observed from peat core data. The net carbon uptake (NCU) represents the modeled carbon that is added to the catotelm at each 100-yr interval. The net carbon release (NCR) represents the total carbon release from the catotelm over time. (b) The peat decomposition modeling (PDM) results from the acrotelm of core DL18-C3. The initial peat mass and initial decay rate were used to calculate the peat mass loss (solid line). Results can be converted to remaining peat carbon (right *y*-axis) to directly compare with NCU (dashed line) in the catotelm.

that the peatland developed into a *Sphagnum*-dominated poor fen or bog with abundant shrubs (mostly Ericaceae). During Stage II–1 (ca. 1450–1700 CE), the high AC values indicate a dry climate, which was widely observed in regional paleoclimate records (Sun et al., 2019; Xiao et al., 2009; Lin et al., 2004). The stalagmite $\delta^{18}O$ values from Dongge Cave (Wang et al., 2005, Fig. 9o) and Shihua Cave (Chu et al., 2012, Fig. 9o) showed relatively positive values that characterize the weakened East Asian summer monsoon and likely drier conditions in northern China (Liu et al., 2014). In addition, the reconstructed Northern Hemisphere temperatures based on multiple tree-ring and proxy records indicate that the lowest temperature over the past two millennia occurred around 1600 CE (Moberg et al., 2005, Fig. 9m). The temperature reconstruction curves based on pollen records from nearby regions, such as Amur Basin (Han et al., 2020), Daihai (Xu et al., 2010), and Sihailongwan (Stebich et al., 2015) all suggest that the temperature decreased significantly at this stage. Our data and other paleoclimate records suggest that the climate at this time was overall characterized by cold and dry conditions, a period often known as the Little Ice Age (LIA; 1350–1850 CE in Le Treut et al. (2007)). The FBT occurred during this period based on macrofossil evidence, potentially indicating that due to regional climate and/or other local factors, the ecosystem equilibrium of fen systems was bypassed (see Section 5.2 for details). The dry climate also increased the charcoal abundance in cores DL18-C2 at ca. 1650 CE. During Stage II–2 (ca. 1700–1960 CE), AC and UOM decreased,

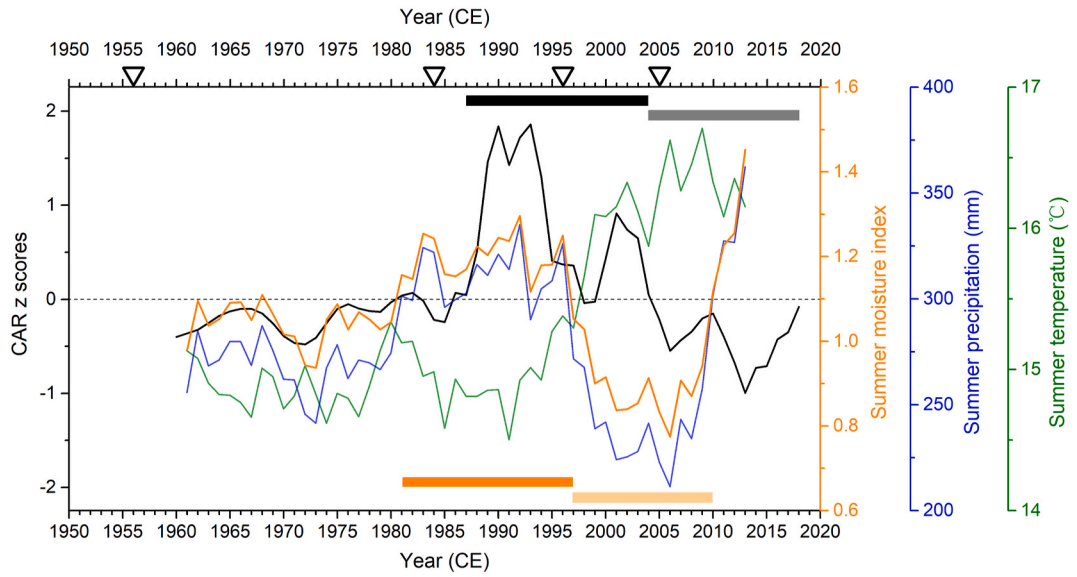

Fig. 8. CAR z scores (representing allogenic CAR) of core DL18-C3 and meteorological data at Arxan station for the period 1961–2013 CE (data from the Meteorological Data Center, China Meteorological Administration at https://data.cma.cn/). CAR z scores, summer moisture index, summer temperature, and summer precipitation are 5-point moving averages. The black rectangle (orange rectangle) shows the period when CAR z scores were >0 (the summer moisture index was greater than the mean value), while the grey rectangle and light orange rectangle represent the opposite. The black triangles on the top indicate the horizons with AMS ^{14}C dates.

indicating a wetter climate (Loisel et al., 2017). The temperature reconstruction records of the Northern Hemisphere (Moberg et al., 2005) and Hulun Lake (Wen et al., 2010) showed a slight increase at this time. The stalagmite $\delta^{18}O$ records from Dongge Cave (Wang et al., 2005) and Shihua Cave (Chu et al., 2012) show relatively negative values, indicating the strengthened East Asian summer monsoon, and pollen-based precipitation records in Hulun Lake (Wen et al., 2010) and the surrounding regions (Han et al., 2020; Xu et al., 2010) all show the trend towards wetter conditions. The warm and wet climate may promote vegetation growth at Darbin Lake peatland, and consequently, the peat accumulation rates were slightly increased as *Sphagnum* mosses and ligneous litter after FBT are more resistant to decomposition than herbaceous plants (Straková et al., 2011). The mean value of aCAR in Stage II was 34.7 g C m^{-2} yr^{-1}, showing only a slight increase compared to Stage I.

Stage III (ca. 1960–2018 CE): The peatland became predominated by *Sphagnum* mosses after ca. 1960 CE, indicating that the bog ecosystem was established during this period. With the climate warming (0.29 °C per decade for mean annual temperature and 0.32 °C per decade for mean summer temperature), *Sphagnum* mosses were replaced by other dry-adapted mosses (mainly *Polytrichum strictum*) in core DL18-C1 after ca. 2000 CE. Additionally, the increase in AC and median grain size after 2000 CE (Fig. 5b) indicates either drier conditions that caused elevated aeolian dust transport or enhanced human activities such as road constructions. Furthermore, it is notable that the aCAR increased rapidly to 139.2 g C m^{-2} yr^{-1} during this phase (Fig. 9f). Except for limited decomposition of recently-accumulated peat (Young et al., 2019), this shift was likely caused by vegetation changes (Loisel and Yu, 2013, Fig. 10; see Section 5.3 for details).

5.2. The heterogeneity of the fen ecosystem

Our multi-core results show that fen ecosystems are heterogeneous in terms of both peat properties and ecosystem dynamics even within a single peatland. For peat properties, during the early stage of the peat accumulation, three coring sites that are only 50 m apart were all in the fen phase but dry bulk density (DBD) and organic matter bulk density (OMBD) are characterized by the large variability among different cores during the period ca. 400–1450 CE, mainly because core DL18-C3 had much higher values than cores DL18-C1 and DL18-C2 (Table 4). Bulk density, as a proxy of peat decomposition and degree of humification, is influenced by factors such as mineral input, peat type, decomposition time, and decomposition condition (Loisel et al., 2014; Yu et al., 2003a). Among these factors, three cores did not show significant differences in ash content and were all predominated by herbaceous plants. Therefore, the higher DBD and OMBD in core DL18-C3 were likely associated with stronger peat decomposition, which was partly supported by the slightly higher unidentifiable organic matter in this core. This may be related to the fact that core DL18-C3 is closest to the edge of the peatland with a lower water table (Table 1).

The heterogeneity of ecosystem dynamics in fen ecosystems is shown in the various timings and potential influence factors of the subsequent FBT (Fig. 9). For peatlands, the FBT might be trigged by autogenic and allogenic processes. The autogenic mechanism assumes that with the long-term peat accumulation, the peat surface may eventually reach an elevation beyond the influence of the mineral-rich groundwater and fundamentally shift the hydrological and nutrient conditions of the peatland into a state of ombrotrophy (Kuhry et al., 1993; Väliranta et al., 2016). The allogenic mechanism assumes that the FBT is likely triggered by external forcings such as hydroclimate changes (Kolari et al., 2022; Loisel and Bunsen, 2020; Tahvanainen, 2011). The transitions into bog vegetation such as *Sphagnum* mosses and shrubs occurred at different times since ca. 1450 CE but within the same time window of LIA. At this interval, the fen ecosystem stability at Darbin Lake peatland was likely lost under the influence of the cold and dry climate. This ecosystem transition was also observed at Tuqiang peatland in the same region (Li et al., 2022), confirming the extensive influence of regional climate on FBT. However, even in the same regional climate context, local environmental variations may lead to asynchronous ecosystem responses for different locations within a peatland (Magnan et al., 2021; Piilo et al., 2020; Väliranta et al., 2016). Although we cannot exclude the importance of autogenic processes, based on our multi-proxy data we suggest three specific potential influence factors for the allogenically-induced, asynchronous FBT: local hydrology, permafrost activity, and fire disturbance.

For local hydrology, we found that core DL18-C3, which has the lowest water table and much higher DBD than other cores, was the earliest to undergo FBT. As the higher DBD may lead to the reduced

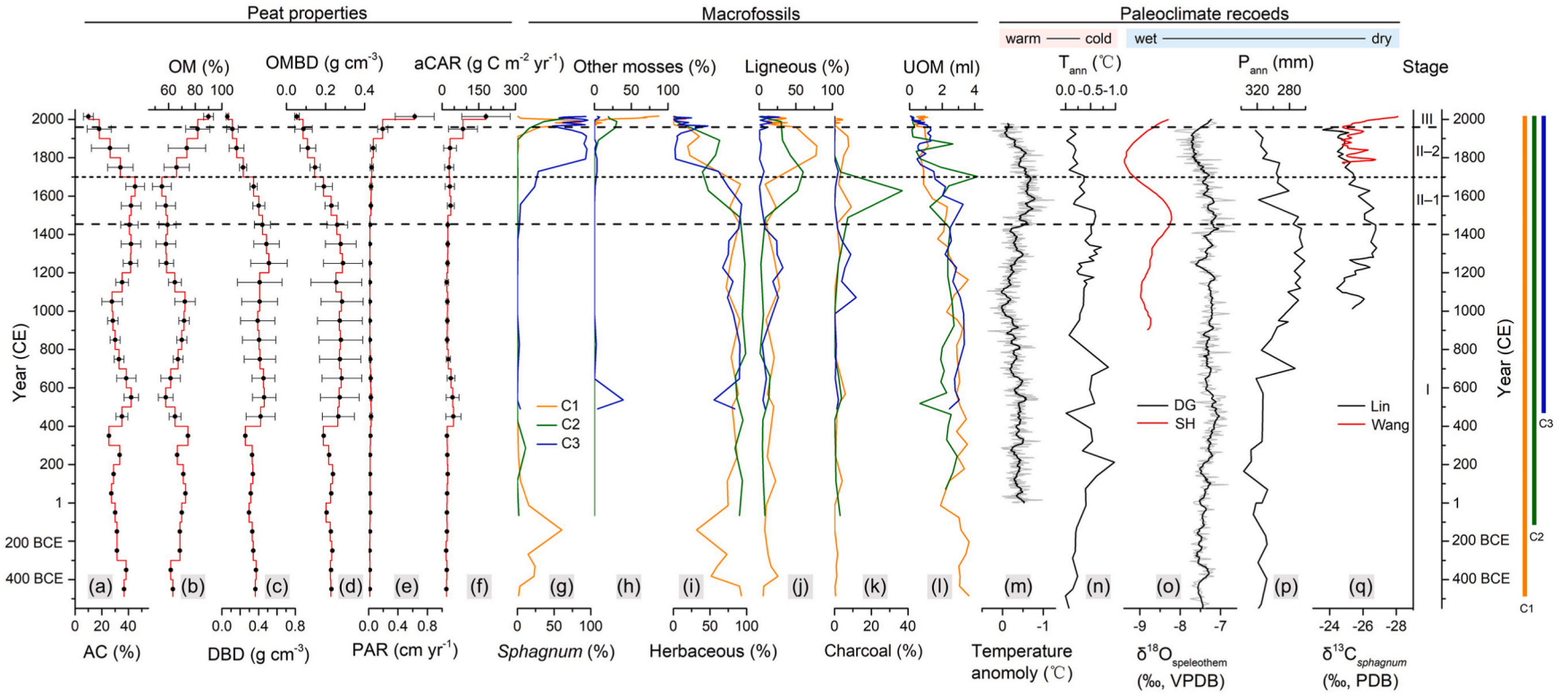

Fig. 9. Comparisons of peat properties (a–f) and macrofossils results (g–l) at Darbin Lake peatland and other paleoclimate records (m–q). (m) The temperature anomaly during the past 2000 years for the Northern Hemisphere (Moberg et al., 2005). (n) The annual temperature (T_{ann}) based on pollen records from Hulun Lake (Wen et al., 2010). (o) The speleothem $\delta^{18}O$ from Dongge Cave (Wang et al., 2005) and Shihua Cave (Chu et al., 2012). (p) The annual precipitation (P_{ann}) based on pollen records from Hulun Lake (Wen et al., 2010). (q) The *Sphagnum* $\delta^{13}C$ (Lin et al., 2004) and the *Sphagnum* stem $\delta^{13}C$ (Wang, 2021) records from Motianling peatland. The color rectangles on the right represent the time spans of three cores.

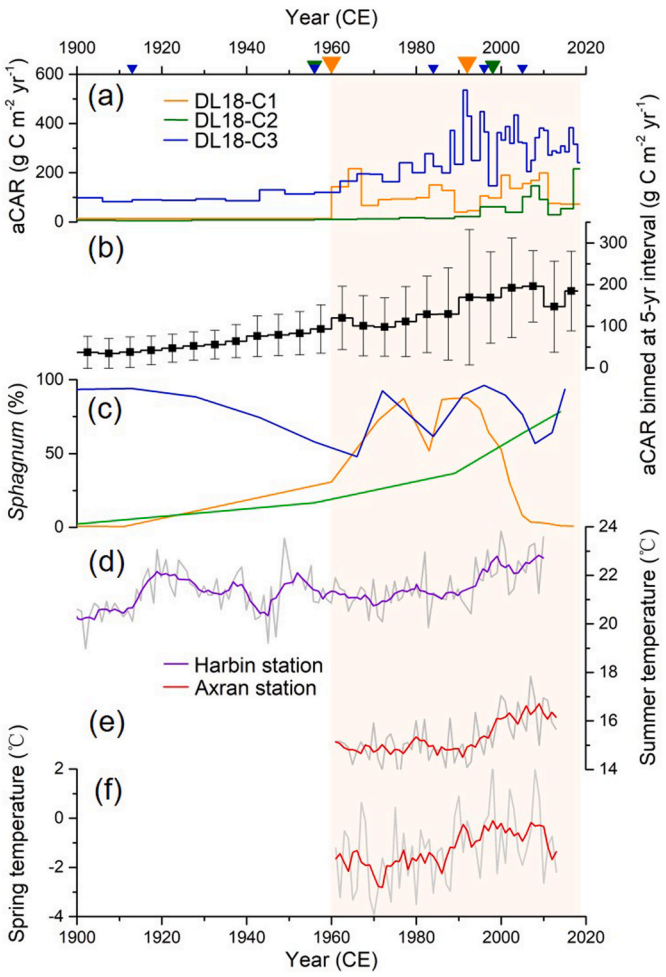

Fig. 10. Comparisons of increasing aCAR, *Sphagnum* abundance and climate warming in the 20th century, including (a) aCAR of each core, (b) mean aCAR of three cores binned at 5-yr interval, (c) abundance of *Sphagnum* macrofossils of each core, summer temperature at (d) Harbin station from the period 1900–2010 CE (Zhang et al., 2011) and (e) Arxan station from the period 1961–2013 CE (data from Meteorological Data Center, China Meteorological Administration at https://data.cma.cn/), and (f) spring temperature at Axran station from the period 1961–2013 CE. The colored lines in (d–f) are 5-point moving averages. The orange, green, and blue triangles on the top indicate the horizons of AMS ^{14}C dates from three cores.

hydraulic conductivity of peat (Morris et al., 2022), we speculate that such conditions might efficiently induce the separation of peatland surface from the influence of mineral-rich groundwater, creating suitable hydrological and nutrient conditions for *Sphagnum* mosses to grow at earliest timing relative to other two cores. This process is often known as the "dry route" of FBT (Loisel and Bunsen, 2020). For permafrost activity, we hypothesize that the peat surface may be drier due to permafrost aggradation and peat expansion during the LIA (Jin et al., 2016). This process may promote peatland transition from wet fens to dry bogs and has been documented in other permafrost-affected peatlands (Magnan et al., 2018b). However, the permafrost aggradation within a peatland is typically asynchronous due to variations in local conditions such as dominant vegetation, microtopography, wind, and sun exposure (Magnan et al., 2021). This heterogeneity may result in the transition of dominant vegetation at cores DL18-C1 and DL18-C2 from wetter fen sedge to drier bog shrubs at different times (ca. 1650 CE and 1500 CE, respectively). For fire disturbance (Väliranta et al., 2016), we found two charcoal peaks between ca. 1050 and 1450 CE at core DL18-C3 before the FBT (Fig. 9k). Fire burning could remove surface vegetation and may promote the colonization and growth of *Sphagnum* by increasing available light (Fenton and Bergeron, 2006; Magnan et al., 2018a) or by increasing decomposition (Vitt and Wieder, 2008) that indirectly affects local hydrology. However, it should be noted that fire may also lead to the reversal from bogs to fens. For example, at core DL18-C2, after the charcoal peak at ca. 1650 CE, the herbaceous plants increased, showing a short-term return to fen features (Magnan et al., 2012).

5.3. Rapid increase in aCAR during last several decades

Northern peatlands have experienced rapid increases in carbon accumulation rates in the acrotelm (Loisel and Yu, 2013; Zhang et al., 2018a), in part because the acrotelm peat has experienced a lesser degree of decomposition (Young et al., 2019, 2021). We observed that the time-weighted mean aCAR increased rapidly to 139.2 g C m^{-2} yr^{-1} during the last several decades, compared to the long-term value of 32.4 g C m^{-2} yr^{-1} for three cores at Darbin Lake peatland. However, when taking the differential decomposition history in peat deposits into consideration (Payne et al., 2019; Young et al., 2019), we found that the carbon sequestration capacity of this peatland was indeed increasing.

The results of exponential decay model showed that the peat accumulation pattern of core DL18-C2 changed from convex in the catotelm to concave in the acrotelm (Fig. 6a), suggesting that peat accumulation is accelerating in the acrotelm (ca. 1750 CE) after the peat accumulation became slower in the catotelm (Yu et al., 2003b). For core DL18-C3 (Fig. 6c–e), the peat decomposition model results showed that after 60-year and 300-year acrotelm decomposition, the remaining peat carbon from an initial annual production of 726 g OM m^{-2} (or 363 g C m^{-2}) is still 231 g C m^{-2} and 94.5 g C m^{-2}, which would still be higher than the modeled catotelm net carbon uptake value simulated from carbon flux reconstruction model (69.2 g C m^{-2} yr^{-1}; Fig. 7b), indicating that the relatively high carbon accumulation rates over the last several decades were not entirely due to the limited decomposition of recently-accumulated peat. Instead, this peatland has recently become a stronger carbon sink than it was in the past.

Although three modeling approaches provide a way to link short-term acrotelm carbon dynamics and long-term catotelm carbon dynamics in peatlands (Bunsen and Loisel, 2020; Loisel and Yu, 2013), we also need to acknowledge that the methodology itself carries uncertainties. First, the selection of the acrotelm/catotelm boundary based on peat core data is subjective. Second, the decomposition rate slows as decomposition progresses in the original peat decomposition model (Frolking et al., 2001), but in three modeling approaches, the decomposition rate is assumed to be constant.

Warming would be expected to promote the carbon accumulation rates and increase the carbon sink capacity of peatlands in high latitudes because of the increasing growing season length and net primary productivity of peat-forming plants (Charman et al., 2013; Gallego-Sala et al., 2018; Zhang et al., 2018a). However, we found that the aCAR did not show a similar trend with summer temperature fluctuations before

Table 4
The difference in bulk density among three cores during the period 400–1450 CE and 1450–2018 CE. DBD: dry bulk density; OMBD: organic matter bulk density.

DBD					OMBD				
Period (CE)	C1	C2	C3	Mean	Period (CE)	C1	C2	C3	Mean
400–1450	0.302	0.354	0.658	0.438	400–1450	0.205	0.206	0.411	0.274
1450–2018	0.252	0.234	0.269	0.251	1450–2018	0.153	0.122	0.189	0.154

ca. 1960 CE (Fig. 10a and d). Rather, we found a close link between aCAR and *Sphagnum* abundance in three cores that explains the pattern of recent aCAR (Fig. 10a–c). For DL18-C1, the *Sphagnum* percentage first increased at ca. 1900 CE, reached maximum at ca. 1960–2000 CE, and then decreased toward the core top. The aCAR was very low before 1960 CE, increased after 1960 CE, and then decreased slightly after 2010 CE, showing a very similar pattern. For DL18-C2, *Sphagnum* percentage increased slowly since ca. 1900 CE and reached the maximum only close to the core top. The aCAR also tracked this gradually increasing trend and became high only after ca. 2000 CE. For DL18-C3, the *Sphagnum* community was established much earlier than 1900 CE and its macrofossil percentage was close to 100%, much higher than the other two cores. As a result, aCAR was indeed much higher than other cores. Despite the fluctuation of *Sphagnum* percentage after 1900 CE, aCAR overall mainly increased due to autogenic processes that have been corrected to extract "allogenic CAR" (see Section 5.4 for details). Therefore, the dramatic increase in aCAR during the last several decades was likely due to the increasing *Sphagnum* abundance and the resultant low decomposition rates of *Sphagnum*-derived litter. When the *Sphagnum* bog was gradually established, on the one hand, *Sphagnum* litter was more resistant to microbial decomposition than vascular plants due to recalcitrant tissues and more abundant phenolic compounds (Loisel et al., 2012; van Breemen, 1995). On the other hand, *Sphagnum* also slowed down vascular plants' growth and inhibited microbial decomposition by creating an environment of high acidity, low nutrient availability, low temperature, and anoxic conditions (Malmer et al., 2003; van Breemen, 1995). The recent colonization or expansion of *Sphagnum* mosses and the consequent increase in carbon accumulation rates have been observed in northern peatlands worldwide (Granlund et al., 2022; Loisel and Yu, 2013; Magnan et al., 2021; Robitaille et al., 2021).

After the 1990s CE, rapidly increasing summer temperature should have indirectly contributed to the increase in recent carbon accumulation rates by providing higher growing season temperatures to promote *Sphagnum* growth (Fig. 10a–e; Dorrepaal et al., 2003; Loisel et al., 2012; Magnan et al., 2021; Primeau and Garneau, 2021). Meanwhile, spring warming also led to earlier snowmelt and longer growing season length (Fig. 10f), which encourages *Sphagnum* mosses to take full advantage of the high light levels and water availability together with increasing air temperature to induce the earlier onset of photosynthetic activity (Aurela et al., 2004; Helbig et al., 2022; Loisel and Yu, 2013). Previous studies have shown that increased nitrogen deposition could promote *Sphagnums* growth (Vitt et al., 2003) and carbon accumulation rates (Turunen et al., 2004) or have the opposite effect (Gunnarsson and Rydin, 2000). However, the nitrogen deposition probably has little effect in this region because the nitrogen deposition rate was less than 0.25 g N m^{-2} yr^{-1} over the recent past (Gu et al., 2016). In summary, the effect of increasing temperature on aCAR after 1990s CE cannot be excluded.

Our records show that there was a synchronous positive trend in the *Sphagnum* growth and rapid carbon accumulation during the late stage of the bog phase at Darbin Lake peatland even though the carbon accumulation is complicated by many control factors (Yu et al., 2009), which suggests that *Sphagnum*, as an important peat-forming plant, plays an important role in carbon accumulation of peatlands, and is the key to high carbon sink capacity of peatland ecosystems (Dorrepaal et al., 2003; Loisel and Bunsen, 2020; Loisel and Yu, 2013; Magnan et al., 2021; Piilo et al., 2023; Taylor et al., 2019).

5.4. Response of allogenic CAR to climate change during the last several decades

Since meteoric water is the main water source for *Sphagnum*-dominated ombrotrophic bogs, the surface moisture and water level of bogs are closely related to the regional effective moisture balance controlled by precipitation and temperature (Charman, 2007; Heijmans et al., 2013; Loisel and Garneau, 2010; Väliranta et al., 2016), both of which are the important factors for vegetation succession and carbon dynamics in peatlands (Piilo et al., 2019; Zhang et al., 2018b, 2020). We used core DL18-C3 to explore the effects of recent climate change during the instrumental period on carbon accumulation rates of the ombrotrophic bog.

Our results show a sensitive response of allogenic CAR to regional summer effective moisture controlled by summer precipitation amount on decadal timescales, while the role of temperature is not immediately clear (Fig. 8). The increasing allogenic CAR at around the 1990s CE coincides with the period of increase in summer effective moisture. When the summer effective moisture decreased subsequently at around the 2000s CE, allogenic CAR also decreased. The macrofossil results of core DL18-C3 showed that the drying in the 2000s CE resulted in a slight increase in woody and herbaceous plants (Tuittila et al., 2012). This may be related to the moisture stress of *Sphagnum* caused by a combination of rising temperatures and lower water table, tipping the competitive advantage from *Sphagnum* mosses to vascular plants that can use deeper water sources (Dieleman et al., 2015). In addition, we found that the timing of changes in allogenic CAR lagged behind the changes in effective moisture, which might indicate that bog plants have a delayed response to hydroclimate changes (Kokkonen et al., 2019; Sim et al., 2021) or be caused by age uncertainties. We attempted to analyze the correlation between CAR z scores and summer moisture index while considering a time lag, and found a significant positive correlation between them ($r = 0.66$, $p < 0.001$; the result is not displayed).

Both temperature and effective moisture conditions affect the balance between plant production and organic matter decomposition, and thus the capacity of peatland carbon sinks. For example, the decrease of effective moisture can accelerate peat decomposition due to exposure to aerobic conditions that reduce the carbon accumulation rate (Swindles et al., 2019). Based on our records, we suggest that the factor of summer precipitation is more important in places like Northeast China where moisture availability is more limited due to continental climates compared to their counterparts in oceanic or monsoonal regions. Indeed, the climate condition of our study sites (MAT = −2.7 °C, MAP = 440 mm) is close to the lower bound of precipitation boundary in the climate space of northern peatlands (Yu et al., 2009). Our results may also suggest that summer precipitation will become an important factor in predicting the future carbon dynamics in northern peatlands in continental interiors (Zhang et al., 2020).

6. Conclusion

In this study, we documented the peatland development and carbon accumulation history at Darbin Lake peatland to understand their responses to past climate changes during the last 2500 years. The results showed that the peatland was initially characterized by a sedge-dominated fen, then changed to a *Sphagnum*-dominated poor fen or bog with abundant shrubs (mostly Ericaceae), and finally became predominated by *Sphagnum* mosses during last several decades. Multi-core analysis indicated that fens are highly heterogeneous in terms of peat properties and ecosystem dynamics even within a single peatland. The rapid increases in aCAR in recent decades might have resulted from the increasing *Sphagnum* abundance and resultant low decomposition of *Sphagnum*-derived litter rather than limited decomposition of recently-accumulated peat, suggesting the important role of vegetation changes in controlling the carbon accumulation rates of northern peatlands. Under the influence of climate warming, the increase in allogenic CAR around the 1990s CE coincides with the period of increased regional summer effective moisture controlled by summer monsoon precipitation, revealing the high sensitivity of ombrotrophic bog ecosystems to hydroclimate changes at decadal timescales. Therefore, moisture availability is likely the more important factor than temperature in predicting the future carbon sink capacity in northern peatlands that are limited by moisture availability.

Funding source

This work was supported by the National Natural Science Foundation of China (NSFC) grants 41877458 and 42330509 to Z. Yu.

Author contribution statement

Z. Yu and Y. Xia conceived the study. Y. Xia conducted most of the lab analysis while Z. Yang contributed to the macrofossil and LOI analysis of core DL18-C2. Z. Yu and Y. Xia analyzed and interpreted the data while J. Sun participated in the discussion of the carbon flux reconstruction model. Y. Xia wrote the initial manuscript. Z. Xia and Z. Yu edited the manuscript.

Declaration of competing interest

The authors declare that they have no known competing financial interests or personal relationships that could have appeared to influence the work reported in this paper.

Data availability

Data will be made available on request.

Acknowledgements

We thank Kunshan Bao, Yan Chen, Yuwen Fu, Zuo Wang, Wei Xing, and Mingming Zhang for field assistance; Yanmin Dong and Hongchun Li for AMS ^{14}C dating analysis; Yuhan Yang, Ruotong Zhao and Xinyue Zhang for part of LOI analysis; Wenkai Liu and Li Wang for discussion of the exponential decay model; Shan Cong for assistance with local knowledge, and two anonymous reviewers for constructive comments.

Appendix A

The exponential decay model (EDM; Clymo, 1984) was used to derive peat addition rate (p) and peat decay coefficient (α) for catotelm (p_c, α_c) and acrotelm (p_a, α_a) by fitting the observed cumulative peat mass data with single exponential decay function, assuming that p and α remain constant over time. These values were then used to drive the following two models. The carbon flux reconstruction model (CFM; Yu, 2011) was used to back-calculate the initial carbon uptake in the catotelm, which was estimated at 100-yr intervals. The peat decomposition model (PDM; Frolking et al., 2001) was used to simulate the remaining peat after the initial peat had decomposed for a certain period of time in the acrotelm. In other words, this is the amount of peat that was thought likely to be transferred to catotelm at that time. Once multiplied by 50%, the result is equivalent to the carbon uptake in the catotelm. Since we could only derive p and α for both acrotelm and catotelm from core DL18-C3, we only discussed the connections between short- and long-term carbon dynamics based on the results of that core. The formula and explanation of terms for three models are shown in Table A1.

Table A1
The formula and explanation of terms for three models.

Model	Formula	Explanation
Exponential decay model (EDM)	$\frac{dM}{dt} = p - \alpha * M$, which has an analytical solution as: $M = \frac{p}{\alpha} * (1 - e^{-\alpha * t})$	M—observed cumulative peat mass; t—time; p—peat addition rate; α—peat decay coefficient.
Carbon flux reconstruction model (CFM)	$NCU_t = \frac{NCP_t}{e^{-\alpha * t}}$, $_{initiation}$ $NCR_t = \sum_{k=t}^{age} \left(\frac{NCP_k}{e^{-\alpha * t}} - \frac{NCP_k}{e^{-\alpha * (t-1)}}\right)$	NCP—observed net C pool from peat core data at the present at each time interval (e.g. 100-yr binned interval in this study); NCU—modeled net carbon uptake from observed NCP by considering and adding total carbon release/loss since the formation of the 100-year peat cohort using the modeled decomposition (fractional mass loss) rate; NCR—total net carbon release from the entire peatland at every 100-yr interval; t—time; α—peat decay coefficient; k—the peat cohort ID to track all peat cohorts older than time t since the initiation of the peatland.
Peat decomposition model (PDM)	$M_t = \frac{M_0}{1 + k_0 t} = \frac{p}{1 + \alpha t}$	M_t—remaining peat at time t; M_0—initial peat mass produced in a year, assuming to be equal to p*1 yr in EDM; k_0—initial decay rate, assuming to be equal to α in EDM; t—time.

References

Archibald, S., Roy, D.P., Wilgen, B.W.V., Scholes, R.J., 2009. What limits fire? An examination of drivers of burnt area in Southern Africa. Global Change Biol. 15, 613–630. https://doi.org/10.1111/j.1365-2486.2008.01754.x.

Aurela, M., Laurila, T., Tuovinen, J., 2004. The timing of snow melt controls the annual CO_2 balance in a subarctic fen. Geophys. Res. Lett. 31, L16119 https://doi.org/10.1029/2004GL020315.

Bao, K., Jia, L., Lu, X., Wang, G., 2010. Grain-size characteristics of sediment in Daniugou peatland in Changbai Mountains, Northeast China: implications for atmospheric dust deposition. Chin. Geogr. Sci. 20, 498–505. https://doi.org/10.1007/s11769-010-0427-z.

Bao, K., Wang, G., Xing, W., Shen, J., 2015. Accumulation of organic carbon over the past 200 years in alpine peatlands, northeast China. Environ. Earth Sci. 73, 7489–7503. https://doi.org/10.1007/s12665-014-3922-1.

Bao, K., Xing, W., Yu, X., Zhao, H., McLaughlin, N., Lu, X., Wang, G., 2012. Recent atmospheric dust deposition in an ombrotrophic peat bog in Great Hinggan Mountain, Northeast China. Sci. Total Environ. 431, 33–45. https://doi.org/10.1016/j.scitotenv.2012.05.014.

Bao, K., Zhao, H., Xing, W., Lu, X., McLaughlin, N.B., Wang, G., 2011. Carbon accumulation in temperate wetlands of Sanjiang Plain, Northeast China. Soil Sci. Soc. Am. J. 75, 2386–2397. https://doi.org/10.2136/sssaj2011.0157.

Blaauw, M., Christen, J.A., 2011. Flexible paleoclimate age-depth models using an autoregressive gamma process. Bayesian Anal. 6, 457–474. https://doi.org/10.1214/11-BA618.

Brown, J., Ferrians, O., Heginbottom, J.A., Melnikov, E., 2002. Circum-Arctic Map of Permafrost and Ground-Ice Conditions. National Snow and Ice Data Center, Boulder, Colorado USA. Version 2 [Data Set]. https://doi.org/10.7265/skbgkf16.

Bunsen, M., Loisel, J., 2020. Carbon storage dynamics in peatlands: comparing recent- and long-term accumulation histories in southern Patagonia. Global Change Biol. 26, 5778–5795 https://doi.org/10.1111/gcb.15262.

Chambers, F.M., Beilman, D.W., Yu, Z., 2011. Methods for determining peat humification and for quantifying peat bulk density, organic matter and carbon content for palaeostudies of climate and peatland carbon dynamics. Mires Peat 7, 1–10.
Charman, D.J., 2007. Summer water deficit variability controls on peatland water-table changes: implications for Holocene palaeoclimate reconstructions. Holocene 17, 217–227. https://doi.org/10.1177/0959683607075836.
Charman, D.J., Beilman, D.W., Blaauw, M., Booth, R.K., Brewer, S., Chambers, F.M., Christen, J.A., Gallego-Sala, A., Harrison, S.P., Hughes, P.D.M., Jackson, S.T., Korhola, A., Mauquoy, D., Mitchell, F.J.G., Prentice, I.C., van der Linden, M., De Vleeschouwer, F., Yu, Z.C., Alm, J., Bauer, I.E., Corish, Y.M.C., Garneau, M., Hohl, V., Huang, Y., Karofeld, E., Le Roux, G., Loisel, J., Moschen, R., Nichols, J.E., Nieminen, T.M., MacDonald, G.M., Phadtare, N.R., Rausch, N., Sillasoo, Ü., Swindles, G.T., Tuittila, E.S., Ukonmaanaho, L., Väliranta, M., van Bellen, S., van Geel, B., Vitt, D.H., Zhao, Y., 2013. Climate-related changes in peatland carbon accumulation during the last millennium. Biogeosciences 10, 929–944. https://doi.org/10.5194/bg-10-929-2013.
Chen, F., Yu, Z., Yang, M., Ito, E., Wang, S., Madsen, D.B., Huang, X., Zhao, Y., Sato, T., John, B., Birks, H., Boomer, I., Chen, J., An, C., Wünnemann, B., 2008. Holocene moisture evolution in arid central Asia and its out-of-phase relationship with Asian monsoon history. Quat. Sci. Rev. 27, 351–364. https://doi.org/10.1016/j.quascirev.2007.10.017.
Chu, P.C., Li, H.C., Fan, C., Chen, Y.H., 2012. Speleothem evidence for temporal–spatial variation in the East Asian summer monsoon since the Medieval Warm Period. J. Quat. Sci. 27, 901–910. https://doi.org/10.1002/jqs.2579.
Clymo, R.S., 1984. The limits to peat bog growth. Phil. Trans. Roy. Soc. Lond. B 303, 605–654. https://doi.org/10.1098/rstb.1984.0002.
Dieleman, C.M., Branfireun, B.A., McLaughlin, J.W., Lindo, Z., 2015. Climate change drives a shift in peatland ecosystem plant community: implications for ecosystem function and stability. Global Change Biol. 21, 388–395. https://doi.org/10.1111/gcb.12643.
Dorrepaal, E., Aerts, R., Cornelissen, J.H.C., Callaghan, T.V., van Logtestijn, R.S.P., 2003. Summer warming and increased winter snow cover affect *Sphagnum fuscum* growth, structure and production in a sub-arctic bog. Global Change Biol. 10, 93–104. https://doi.org/10.1046/j.1529-8817.2003.00718.x.
Dorrepaal, E., Toet, S., van Logtestijn, R.S.P., Swart, E., van de Weg, M.J., Callaghan, T.V., Aerts, R., 2009. Carbon respiration from subsurface peat accelerated by climate warming in the subarctic. Nature 460, 616–619. https://doi.org/10.1038/nature08216.
Fenton, N.J., Bergeron, Y., 2006. Facilitative succession in a boreal bryophyte community driven by changes in available moisture and light. J. Veg. Sci. 17, 65–76. https://doi.org/10.1111/j.1654-1103.2006.tb02424.x.
Friedlingstein, P., Cox, P., Betts, R., Bopp, L., von Bloh, W., Brovkin, V., Cadule, P., Doney, S., Eby, M., Fung, I., Bala, G., John, J., Jones, C., Joos, F., Kato, T., Kawamiya, M., Knorr, W., Lindsay, K., Matthews, H.D., Raddatz, T., Rayner, P., Reick, C., Roeckner, E., Schnitzler, K.G., Schnur, R., Strassmann, K., Weaver, A.J., Yoshikawa, C., Zeng, N., 2006. Climate–carbon cycle feedback analysis: results from the C⁴MIP model intercomparison. J. Clim. 19, 3337–3353. https://doi.org/10.1175/JCLI3800.1.
Frolking, S., Roulet, N.T., 2007. Holocene radiative forcing impact of northern peatland carbon accumulation and methane emissions. Global Change Biol. 13, 1079–1088. https://doi.org/10.1111/j.1365-2486.2007.01339.x.
Frolking, S., Roulet, N.T., Moore, T.R., Richard, P.J.H., Lavoie, M., Muller, S.D., 2001. Modeling northern peatland decomposition and peat accumulation. Ecosystems 4, 479–498. https://doi.org/10.1007/s10021-001-0105-1.
Frolking, S., Roulet, N., Tuittila, E., Bubier, J., Quillet, A., Talbot, J., Richard, P., 2010. A new model of Holocene peatland net primary production, decomposition, water balance, and peat accumulation. Earth Syst. Dynam. 1, 1–21. https://doi.org/10.5194/esdd-1-115-2010.
Gallego-Sala, A.V., Charman, D.J., Brewer, S., Page, S.E., Prentice, I.C., Friedlingstein, P., Moreton, S., Amesbury, M.J., Beilman, D.W., Björck, S., Blyakharchuk, T., Bochicchio, C., Booth, R.K., Bunbury, J., Camill, P., Carless, D., Chimner, R.A., Clifford, M., Cressey, E., Courtney-Mustaphi, C., De Vleeschouwer, F., de Jong, R., Fialkiewicz-Koziel, B., Finkelstein, S.A., Garneau, M., Githumbi, E., Hribjlan, J., Holmquist, J., Hughes, P.D.M., Jones, C., Jones, M.C., Karofeld, E., Klein, E.S., Kokfelt, U., Korhola, A., Lacourse, T., Le Roux, G., Lamentowicz, M., Large, D., Lavoie, M., Loisel, J., Mackay, H., MacDonald, G.M., Makila, M., Magnan, G., Marchant, R., Marcisz, K., Martínez Cortizas, A., Massa, C., Mathijssen, P., Mauquoy, D., Mighall, T., Mitchell, F.J.G., Moss, P., Nichols, J., Oksanen, P.O., Orme, L., Packalen, M.S., Robinson, S., Roland, T.P., Sanderson, N.K., Sannel, A.B.K., Silva-Sánchez, N., Steinberg, N., Swindles, G.T., Turner, T.E., Uglow, J., Väliranta, M., van Bellen, S., van der Linden, M., van Geel, B., Wang, G., Yu, Z., Zaragoza-Castells, J., Zhao, Y., 2018. Latitudinal limits to the predicted increase of the peatland carbon sink with warming. Nat. Clim. Change 8, 907–913. https://doi.org/10.1038/s41558-018-0271-1.
Gu, F., Huang, M., Zhang, Y., Yan, H., Li, J., Guo, R., Zhong, X., 2016. Modeling the temporal-spatial patterns of atmospheric nitrogen deposition in China during 1961–2010. Acta Ecol. Sin. 36, 3591–3600 (in Chinese). doi:10.5846/stxb201409211868.
Gunnarsson, U., Rydin, H., 2000. Nitrogen fertilization reduces *Sphagnum* production in bog communities. New Phytol. 147, 527–537. https://doi.org/10.1046/j.1469-8137.2000.00717.x.
Granlund, L., Vesakoski, V., Sallinen, A., Kolari, T.H.M., Wolff, F., Tahvanainen, T., 2022. Recent lateral expansion of *Sphagnum* bogs over central fen areas of boreal aapa mire complexes. Ecosystems 25, 1455–1475. https://doi.org/10.1007/s10021-021-00726-5.
Han, D., Gao, C., Liu, H., Yu, X., Li, Y., Cong, J., Wang, G., 2020. Vegetation dynamics and its response to climate change during the past 2000 years along the Amur River Basin, Northeast China. Ecol. Indicat. 117, 106577 https://doi.org/10.1016/j.ecolind.2020.106577.
Heijmans, M.M.P.D., van der Knaap, Y.A.M., Holmgren, M., Limpens, J., 2013. Persistent versus transient tree encroachment of temperate peat bogs: effects of climate warming and drought events. Global Change Biol. 19, 2240–2250. https://doi.org/10.1111/gcb.12202.
Heiri, O., Lotter, A.F., Lemcke, G., 2001. Loss on ignition as a method for estimating organic and carbonate content in sediments: reproducibility and comparability of results. J. Paleolimnol. 25, 101–110. https://doi.org/10.1023/A:1008119611481.
Helbig, M., Živković, T., Alekseychik, P., Aurela, M., El-Madany, T.S., Euskirchen, E.S., Flanagan, L.B., Griffis, T.J., Hanson, P.J., Hattakka, J., Helfter, C., Hirano, T., Humphreys, E.R., Kiely, G., Kolka, R.K., Laurila, T., Leahy, P.G., Lohila, A., Mammarella, I., Nilsson, M.B., Panov, A., Parmentier, F.J.W., Peichl, M., Rinne, J., Roman, D.T., Sonnentag, O., Tuittila, E.S., Ueyama, M., Vesala, T., Vestin, P., Weldon, S., Weslien, P., Zaehle, S., 2022. Warming response of peatland CO_2 sink is sensitive to seasonality in warming trends. Nat. Clim. Change. https://doi.org/10.1038/s41558-022-01428-z.
Hua, Q., Turnbull, J.C., Santos, G.M., Rakowski, A.Z., Ancapichún, S., De Pol-Holz, R., Hammer, S., Lehman, S.J., Levin, I., Miller, J.B., Palmer, J.G., Turney, C.S.M., 2022. Atmospheric radiocarbon for the period 1950–2019. Radiocarbon 64, 723–745. https://doi.org/10.1017/RDC.2021.95.
Hugelius, G., Loisel, J., Chadburn, S., Jackson, R.B., Jones, M., MacDonald, G., Marushchak, M., Olefeldt, D., Packalen, M., Siewert, M.B., Treat, C., Turetsky, M., Voigt, C., Yu, Z., 2020. Large stocks of peatland carbon and nitrogen are vulnerable to permafrost thaw. Proc. Natl. Acad. Sci. U.S.A. 117, 20438–20446. https://doi.org/10.1073/pnas.1916387117.
Jin, H., Chang, X., Luo, D., He, R., Lü, L., Yang, S., Guo, D., 2016. Evolution of permafrost in Northeast China since the Late Pleistocene. Sci. Cold Arid Reg. 8, 269–296. https://doi.org/10.3724/SP.J.1226.2016.00269.
Jin, H., Li, S., Cheng, G., Wang, S., Li, X., 2000. Permafrost and climatic change in China. Global Planet. Change 26, 387–404. https://doi.org/10.1016/S0921-8181(00)00051-5.
Jones, M.C., Harden, J., O'Donnell, J., Manies, K., Jorgenson, T., Treat, C., Ewing, S., 2017. Rapid carbon loss and slow recovery following permafrost thaw in boreal peatlands. Global Change Biol. 23, 1109–1127. https://doi.org/10.1111/gcb.13403.
Jones, M.C., Yu, Z., 2010. Rapid deglacial and early Holocene expansion of peatlands in Alaska. Proc. Natl. Acad. Sci. U.S.A. 107, 7347–7352. https://doi.org/10.1073/pnas.0911387107.
Kokkonen, N.A.K., Laine, A.M., Laine, J., Vasander, H., Kurki, K., Gong, J., Tuittila, E.S., 2019. Responses of peatland vegetation to 15-year water level drawdown as mediated by fertility level. J. Veg. Sci. 30, 1206–1216. https://doi.org/10.1111/jvs.12794.
Kolari, T.H.M., Sallinen, A., Wolff, F., Kumpula, T., Tolonen, K., Tahvanainen, T., 2022. Ongoing fen–bog transition in a boreal aapa mire inferred from repeated field sampling, aerial images, and landsat data. Ecosystems 25, 1166–1188. https://doi.org/10.1007/s10021-021-00708-7.
Kuhry, P., Nicholson, B.J., Gignac, L.D., Vitt, D.H., Bayley, S.E., 1993. Development of *Sphagnum*-dominated peatlands in boreal continental Canada. Can. J. Bot. 71, 10–22. https://doi.org/10.1139/b93-002.
Le Treut, H., Somerville, R., Cubasch, U., Ding, Y., Mauritzen, C., Mokssit, A., Peterson, T., Prather, M., 2007. Historical overview of climate change science. In: Solomon, S., Qin, D., Manning, M., Chen, Z., Marquis, M., Averyt, K.B., Tignor, M., Miller, H.L. (Eds.), Climate Change 2007: the Physical Science Basis. Contribution of Working Group I to the Fourth Assessment Report of the Intergovernmental Panel on Climate Change. Cambridge University Press, Cambridge, UK and New York, NY, USA, pp. 93–127.
Li, N., Chambers, F.M., Yang, J., Jie, D., Liu, L., Liu, H., Gao, G., Gao, Z., Li, D., Shi, J., Feng, Y., Qiao, Z., 2017. Records of East Asian monsoon activities in Northeastern China since 15.6 ka, based on grain size analysis of peaty sediments in the Changbai Mountains. Quat. Int. 447, 158–169. https://doi.org/10.1016/j.quaint.2017.03.064.
Li, Y., Gao, C., Liu, H., Han, D., Cong, J., Li, X., Wang, G., 2022. Distribution of phosphorus forms in surface soils of typical peatlands in northern Great Khingan Mountains and its potential to reconstruct paleo-vegetations. J. Environ. Manag. 302, 114033 https://doi.org/10.1016/j.jenvman.2021.114033.
Lin, Q., Leng, X., Hong, B., 2004. The peat record of 1ka of climate change in Daxing Anling. Bull. China Soc. Mineral Petrol. Geochem. 23, 15–18 (in Chinese). doi: 10.1088/1009-0630/6/5/011.
Liu, H., Yu, Z., Han, D., Gao, C., Yu, X., Wang, G., 2019. Temperature influence on peatland carbon accumulation over the last century in Northeast China. Clim. Dynam. 53, 2161–2173. https://doi.org/10.1007/s00382-019-04813-1.
Liu, Z., Wen, X., Brady, E., Otto-Bliesner, B., Yu, G., Lu, H., Cheng, H., Wang, Y., Zheng, W., Ding, Y., Edwards, R., Cheng, J., Liu, W., Yang, H., 2014. Chinese cave records and the East asia summer monsoon. Quat. Sci. Rev. 83, 115–128. https://doi.org/10.1016/j.quascirev.2013.10.021.
Loisel, J., Bunsen, M., 2020. Abrupt fen-bog transition across southern Patagonia: timing, causes, and impacts on carbon sequestration. Front. Ecol. Evol. 8, 1–19. https://doi.org/10.3389/fevo.2020.00273.
Loisel, J., Gallego-Sala, A.V., Yu, Z., 2012. Global-scale pattern of peatland *Sphagnum* growth driven by photosynthetically active radiation and growing season length. Biogeosciences 9, 2737–2746. https://doi.org/10.5194/bg-9-2737-2012.
Loisel, J., Garneau, M., 2010. Late Holocene paleoecohydrology and carbon accumulation estimates from two boreal peat bogs in eastern Canada: potential and limits of multi-proxy archives. Palaeogeogr. Palaeoclimatol. Palaeoecol. 291, 493–533. https://doi.org/10.1016/j.palaeo.2010.03.020.

Loisel, J., Yu, Z., 2013. Recent acceleration of carbon accumulation in a boreal peatland, south central Alaska. J. Geophys. Res.: Biogeosciences 118, 41–53. https://doi.org/10.1029/2012JG001978.

Loisel, J., Yu, Z., Beilman, D.W., Camill, P., Alm, J., Amesbury, M.J., Anderson, D., Andersson, S., Bochicchio, C., Barber, K., Belyea, L.R., Bunbury, J., Chambers, F.M., Charman, D.J., De Vleeschouwer, F., Fiałkiewicz-Kozieł, B., Finkelstein, S.A., Gałka, M., Garneau, M., Hammarlund, D., Hinchcliffe, W., Holmquist, J., Hughes, P., Jones, M.C., Klein, E.S., Kokfelt, U., Korhola, A., Kuhry, P., Lamarre, A., Lamentowicz, M., Large, D., Lavoie, M., MacDonald, G., Magnan, G., Mäkilä, M., Mallon, G., Mathijssen, P., Mauquoy, D., McCarroll, J., Moore, T.R., Nichols, J., O Reilly, B., Oksanen, P., Packalen, M., Peteet, D., Richard, P.J., Robinson, S., Ronkainen, T., Rundgren, M., Sannel, A.B.K., Tarnocai, C., Thom, T., Tuittila, E., Turetsky, M., Väliranta, M., van der Linden, M., van Geel, B., van Bellen, S., Vitt, D., Zhao, Y., Zhou, W., 2014. A database and synthesis of northern peatland soil properties and Holocene carbon and nitrogen accumulation. Holocene 24, 1028–1042. https://doi.org/10.1177/0959683614538073.

Loisel, J., Yu, Z., Beilman, D.W., Kaiser, K., Parnikoza, I., 2017. Peatland ecosystem processes in the maritime Antarctic during warm climates. Sci. Rep. 7, 12344 https://doi.org/10.1038/s41598-017-12479-0.

Ma, Z., Fu, C., 2001. Trend of surface humid index in the arid area of Northren China. Acta Meteorol. Sin. 59, 737–746 (in Chinese). doi:10.3321/j.issn:0577-6619.2001.06.010.

MacDonald, G., Beilman, D., Kremenetski, K.V., Sheng, Y., Smith, L., Velichko, A., 2006. Rapid early development of circumarctic peatlands and atmospheric CH_4 and CO_2 variations. Science 314, 285–288. https://doi.org/10.1126/science.1131722.

Magnan, G., Lavoie, M., Payette, S., 2012. Impact of fire on long-term vegetation dynamics of ombrotrophic peatlands in northwestern Québec, Canada. Quat. Res. 77, 110–121. https://doi.org/10.1016/j.yqres.2011.10.006.

Magnan, G., Le Stum-Boivin, É., Garneau, M., Grondin, P., Fenton, N., Bergeron, Y., 2018a. Holocene vegetation dynamics and hydrological variability in forested peatlands of the Clay Belt, eastern Canada, reconstructed using a palaeoecological approach. Boreas 48, 131–146. https://doi.org/10.1111/bor.12345.

Magnan, G., Sanderson, N.K., Piilo, S., Pratte, S., Väliranta, M., van Bellen, S., Zhang, H., Garneau, M., 2021. Widespread recent ecosystem state shifts in high-latitude peatlands of northeastern Canada and implications for carbon sequestration. Global Change Biol. 28, 1919–1934. https://doi.org/10.1111/gcb.16032.

Magnan, G., van Bellen, S., Davies, L., Froese, D., Garneau, M., Mullan-Boudreau, G., Zaccone, C., Shotyk, W., 2018b. Impact of the Little Ice Age cooling and 20th century climate change on peatland vegetation dynamics in central and northern Alberta using a multi-proxy approach and high-resolution peat chronologies. Quat. Sci. Rev. 185, 230–243. https://doi.org/10.1016/j.quascirev.2018.01.015.

Malmer, N., Albinsson, C., Svensson, B.M., Wallén, B., 2003. Interferences between *Sphagnum* and vascular plants: effects on plant community structure and peat formation. Oikos 100, 469–482. https://doi.org/10.1034/j.1600-0706.2003.12170.x.

Mauquoy, D., Hughes, P., van Geel, B., 2010. A protocol for plant macrofossil analysis of peat deposits. Mires Peat 7, 1–5.

Moberg, A., Sonechkin, D.M., Holmgren, K., Datsenko, N.M., Karlén, W., 2005. Highly variable Northern Hemisphere temperatures reconstructed from low- and high-resolution proxy data. Nature 433, 613–617. https://doi.org/10.1038/nature03265.

Morris, P.J., Davies, M.L., Baird, A.J., Balliston, N., Bourgault, M.A., Clymo, R.S., Fewster, R.E., Furukawa, A.K., Holden, J., Kessel, E., Ketcheson, S.J., Kløve, B., Larocque, M., Marttila, H., Menberu, M.W., Moore, P.A., Price, J.S., Ronkanen, A.K., Rosa, E., Strack, M., Surridge, B.W.J., Waddington, J.M., Whittington, P., Wilkinson, S.L., 2022. Saturated hydraulic conductivity in northern peats inferred from other measurements. Water Resour. Res. 58, e2022WR033181 https://doi.org/10.1029/2022WR033181.

Payne, R.J., Ring-Hrubesh, F., Rush, G., Sloan, T.J., Evans, C.D., Mauquoy, D., 2019. Peatland initiation and carbon accumulation in the Falkland Islands. Quat. Sci. Rev. 212, 213–218. https://doi.org/10.1016/j.quascirev.2019.03.022.

Piilo, S.R., Korhola, A., Heiskanen, L., Tuovinen, J., Aurela, M., Juutinen, S., Marttila, H., Saari, M., Tuittila, E., Turunen, J., Väliranta, M.M., 2020. Spatially varying peatland initiation, Holocene development, carbon accumulation patterns and radiative forcing within a subarctic fen. Quat. Sci. Rev. 248, 106596 https://doi.org/10.1016/j.quascirev.2020.106596.

Piilo, S.R., Väliranta, M.M., Amesbury, M.J., Aquino López, M.A., Charman, D.J., Gallego Sala, A., Garneau, M., Koroleva, N., Kärppä, M., Laine, A.M., Sannel, A.B.K., Tuittila, E.S., Zhang, H., 2023. Consistent centennial-scale change in European sub-Arctic peatland vegetation toward *Sphagnum* dominance—implications for carbon sink capacity. Global Change Biol. 29, 1530–1544. https://doi.org/10.1111/gcb.16554.

Piilo, S.R., Zhang, H., Garneau, M., Gallego-Sala, A., Amesbury, M.J., Valiranta, M.M., 2019. Recent peat and carbon accumulation following the Little Ice Age in northwestern Québec, Canada. Environ. Res. Lett. 14, 75002 https://doi.org/10.1088/1748-9326/ab11ec.

Primeau, G., Garneau, M., 2021. Carbon accumulation in peatlands along a boreal to subarctic transect in eastern Canada. Holocene 31, 858–869. https://doi.org/10.1177/0959683620988031.

Reimer, P.J., Austin, W.E.N., Bard, E., Bayliss, A., Blackwell, P.G., Bronk Ramsey, C., Butzin, M., Cheng, H., Edwards, R.L., Friedrich, M., Grootes, P.M., Guilderson, T.P., Hajdas, I., Heaton, T.J., Hogg, A.G., Hughen, K.A., Kromer, B., Manning, S.W., Muscheler, R., Palmer, J.G., Pearson, C., van der Plicht, J., Reimer, R.W., Richards, D.A., Scott, E.M., Southon, J.R., Turney, C.S.M., Wacker, L., Adolphi, F., Büntgen, U., Capano, M., Fahrni, S.M., Fogtmann-Schulz, A., Friedrich, R., Köhler, P., Kudsk, S., Miyake, F., Olsen, J., Reinig, F., Sakamoto, M., Sookdeo, A., Talamo, S., 2020. The IntCal20 Northern Hemisphere radiocarbon age calibration curve (0–55 cal kBP). Radiocarbon 62, 725–757. https://doi.org/10.1017/RDC.2020.41.

Robitaille, M., Garneau, M., van Bellen, S., Sanderson, N.K., 2021. Long-term and recent ecohydrological dynamics of patterned peatlands in north-central Quebec (Canada). Holocene 31, 844–857. https://doi.org/10.1177/0959683620988051.

Ryberg, E.E., Väliranta, M., Martinez Cortizas, A., Ehrlén, J., Sjöström, J.K., Kylander, M. E., 2022. Postglacial peatland vegetation succession in Store Mosse bog, south-central Sweden: an exploration of factors driving species change. Boreas 51, 651–666. https://doi.org/10.1111/bor.12580.

Sim, T.G., Swindles, G.T., Morris, P.J., Baird, A.J., Cooper, C.L., Gallego-Sala, A.V., Charman, D.J., Roland, T.P., Borken, W., Mullan, D.J., Aquino-López, M.A., Gałka, M., 2021. Divergent responses of permafrost peatlands to recent climate change. Environ. Res. Lett. 16, 034001 https://doi.org/10.1088/1748-9326/abe00b.

Sim, T.G., Swindles, G.T., Morris, P.J., Gałka, M., Mullan, D., Galloway, J.M., 2019. Pathways for ecological change in Canadian High Arctic wetlands under rapid twentieth century warming. Geophys. Res. Lett. 46, 4726–4737. https://doi.org/10.1029/2019GL082611.

Stebich, M., Rehfeld, K., Schlütz, F., Tarasov, P.E., Liu, J., Mingram, J., 2015. Holocene vegetation and climate dynamics of NE China based on the pollen record from Sihailongwan Maar Lake. Quat. Sci. Rev. 124, 275–289. https://doi.org/10.1016/j.quascirev.2015.07.021.

Straková, P., Niemi, R.M., Freeman, C., Peltoniemi, K., Toberman, H., Heiskanen, I., Fritze, H., Laiho, R., 2011. Litter type affects the activity of aerobic decomposers in a boreal peatland more than site nutrient and water table regimes. Biogeosciences 8, 2741–2755. https://doi.org/10.5194/bg-8-2741-2011.

Sun, J., Li, H., Wang, J., Zhao, H., Wang, S., Li, H., Yang, Q., Chou, C., Kashyap, S., 2019. Study of Jinchuan Mire in NE China II: peatland development, carbon accumulation and climate change during the past 1000 years. Quat. Int. 528, 18–29. https://doi.org/10.1016/j.quaint.2019.05.007.

Swindles, G.T., Morris, P.J., Mullan, D.J., Payne, R.J., Roland, T.P., Amesbury, M.J., Lamentowicz, M., Turner, T.E., Gallego-Sala, A., Sim, T., Barr, I.D., Blaauw, M., Blundell, A., Chambers, F.M., Charman, D.J., Feurdean, A., Galloway, J.M., Gałka, M., Green, S.M., Kajukało, K., Karofeld, E., Korhola, A., Lamentowicz, A., Langdon, P., Marcisz, K., Mauquoy, D., Mazei, Y.A., McKeown, M.M., Mitchell, E.A. D., Novenko, E., Plunkett, G., Roe, H.M., Schoning, K., Sillasoo, Ü., Tsyganov, A.N., van der Linden, M., Väliranta, M., Warner, B., 2019. Widespread drying of European peatlands in recent centuries. Nat. Geosci. 12, 922–928. https://doi.org/10.1038/s41561-019-0462-z.

Tahvanainen, T., 2011. Abrupt ombrotrophication of a boreal aapa mire triggered by hydrological disturbance in the catchment. J. Ecol. 99, 404–415. https://doi.org/10.1111/j.1365-2745.2010.01778.x.

Taylor, L.S., Swindles, G.T., Morris, P.J., Gałka, M., Green, S.M., 2019. Evidence for ecosystem state shifts in Alaskan continuous permafrost peatlands in response to recent warming. Quat. Sci. Rev. 207, 134–144. https://doi.org/10.1016/j.quascirev.2019.02.001.

Tuittila, E., Juutinen, S., Frolking, S., Väliranta, M., Laine, A.M., Miettinen, A., Seväkivi, M., Quillet, A., Merilä, P., 2012. Wetland chronosequence as a model of peatland development: vegetation succession, peat and carbon accumulation. Holocene 23, 25–35. https://doi.org/10.1177/0959683612450197.

Turunen, J., Roulet, N.T., Moore, T.R., Richard, P.J.H., 2004. Nitrogen deposition and increased carbon accumulation in ombrotrophic peatlands in eastern Canada. Global Biogeochem. Cycles 18, GB3002. https://doi.org/10.1029/2003GB002154.

Väliranta, M., Salojärvi, N., Vuorsalo, A., Juutinen, S., Korhola, A., Luoto, M., Tuittila, E., 2016. Holocene fen–bog transitions, current status in Finland and future perspectives. Holocene 27, 752–764. https://doi.org/10.1177/0959683616670471.

van Breemen, N., 1995. How *Sphagnum* bogs down other plants. Trends Ecol. Evol. 10, 270–275. https://doi.org/10.1016/0169-5347(95)90007-1.

Vitt, D.H., Wieder, R.K., 2008. The structure and function of bryophyte-dominated peatlands. In: Shaw, A.J., Goffinet, B. (Eds.), Bryophyte Biology, second ed. Cambridge University Press, Cambridge, UK and New York, NY, USA, pp. 357–392. https://doi.org/10.1017/CBO9780511754807.010.

Vitt, D.H., Wieder, K., Halsey, L.A., Turetsky, M., 2003. Response of *Sphagnum fuscum* to nitrogen deposition: a case study of ombrogenous peatlands in Alberta, Canada. Bryologist 106, 235–245. https://doi.org/10.2307/3244658.

Wang, M., Yang, G., Gao, Y., Chen, H., Wu, N., Peng, C., Zhu, Q., Zhu, D., Wu, J., He, Y., Tian, J., Zhao, X., Zhang, Y., 2015. Higher recent peat C accumulation than that during the Holocene on the Zoige Plateau. Quat. Sci. Rev. 114, 116–125. https://doi.org/10.1016/j.quascirev.2015.01.025.

Wang, X., Xiao, J., Cui, L., Ding, Z., 2013. Holocene changes in fire frequency in the Daihai Lake region (north-central China): indications and implications for an important role of human activity. Quat. Sci. Rev. 59, 18–29. https://doi.org/10.1016/j.quascirev.2012.10.033.

Wang, Y., Cheng, H., Edwards, R.L., He, Y., Kong, X., An, Z., Wu, J., Kelly, M.J., Dykoski, C.A., Li, X., 2005. The Holocene Asian monsoon: links to solar changes and North Atlantic climate. Science 308, 854–857. https://doi.org/10.1126/science.1106296.

Wang, Z., 2021. Atmospheric Circulation, Hydroclimate Change, and Peat Accumulation over the Last 250 Years Inferred from a *Sphagnum* Peatland in the Middle Greater Khingan Mountains of Northeast China. M.S. Thesis, Northest Normal University, Changchun, China. doi:10.27011/d.cnki.gdbsu.2021.001173.

Wen, R., Xiao, J., Chang, Z., Zhai, D., Xu, Q., Li, Y., Itoh, S., 2010. Holocene precipitation and temperature variations in the East Asian monsoonal margin from pollen data from Hulun Lake in northeastern Inner Mongolia, China. Boreas 39, 262–272. https://doi.org/10.1111/j.1502-3885.2009.00125.x.

Xiao, J., Chang, Z., Si, B., Qin, X., Itoh, S., Lomtatidze, Z., 2009. Partitioning of the grain-size components of Dali Lake core sediments: evidence for lake-level changes during the Holocene. J. Paleolimnol. 42, 249–260. https://doi.org/10.1007/s10933-008-9274-7.

Xing, W., 2017. Carbon Accumulation in Wetlands Sediments, Northeast China Ph.D. Thesis Northeast Institute of Geography and Agroecology. Chinese Academy of Sciences, Changchun, China.

Xing, W., Bao, K., Gallego-Sala, A.V., Charman, D.J., Zhang, Z., Gao, C., Lu, X., Wang, G., 2015. Climate controls on carbon accumulation in peatlands of Northeast China. Quat. Sci. Rev. 115, 78–88. https://doi.org/10.1016/j.quascirev.2015.03.005.

Xu, Q., Xiao, J., Li, Y., Tian, F., Nakagawa, T., 2010. Pollen-based quantitative reconstruction of Holocene climate changes in the Daihai Lake area, Inner Mongolia, China. J. Clim. 23, 2856–2868. https://doi.org/10.1175/2009JCLI3155.1.

Yang, Q., Liu, Z., Bai, E., 2023. Comparison of carbon and nitrogen accumulation rate between bog and fen phases in a pristine peatland with the fen-bog transition. Global Change Biol. 29, 1–17. https://doi.org/10.1111/gcb.16915.

Young, D.M., Baird, A.J., Charman, D.J., Evans, C.D., Gallego-Sala, A.V., Gill, P.J., Hughes, P.D.M., Morris, P.J., Swindles, G.T., 2019. Misinterpreting carbon accumulation rates in records from near-surface peat. Sci. Rep. 9, 17939 https://doi.org/10.1038/s41598-019-53879-8.

Young, D.M., Baird, A.J., Gallego-Sala, A.V., Loisel, J., 2021. A cautionary tale about using the apparent carbon accumulation rate (aCAR) obtained from peat cores. Sci. Rep. 11, 9547. https://doi.org/10.1038/s41598-021-88766-8.

Yu, Z., 2011. Holocene carbon flux histories of the world's peatlands. Holocene 21, 761–774. https://doi.org/10.1177/0959683610386982.

Yu, Z., 2012. Northern peatland carbon stocks and dynamics: a review. Biogeosciences 9, 4071–4085. https://doi.org/10.5194/bg-9-4071-2012.

Yu, Z., Beilman, D.W., Jones, M.C., 2009. Sensitivity of northern peatland carbon dynamics to Holocene climate change. In: Baird, A.J., Belyea, L.R., Comas, X., Reeve, A.S., Slater, L.D. (Eds.), Geophys. Monogr. Ser: Carbon Cycling in Northern Peatlands. Am. Geophys. Union, Washington, DC, pp. 55–69. https://doi.org/10.1029/2008GM000822.

Yu, Z., Campbell, I.D., Campbell, C., Vitt, D.H., Bond, G.C., Apps, M.J., 2003a. Carbon sequestration in western Canadian peat highly sensitive to Holocene wet-dry climate cycles at millennial timescales. Holocene 13, 801–808. https://doi.org/10.1191/0959683603hl667ft.

Yu, Z., Loisel, J., Brosseau, D.P., Beilman, D.W., Hunt, S.J., 2010. Global peatland dynamics since the Last Glacial Maximum. Geophys. Res. Lett. 37, L13402 https://doi.org/10.1029/2010GL043584.

Yu, Z., Vitt, D.H., Campbell, I.D., Apps, M.J., 2003b. Understanding Holocene peat accumulation pattern of continental fens in western Canada. Can. J. Bot. 81, 267–282. https://doi.org/10.1139/b03-016.

Zhang, H., Gallego-Sala, A.V., Amesbury, M.J., Charman, D.J., Piilo, S.R., Väliranta, M. M., 2018a. Inconsistent response of Arctic permafrost peatland carbon accumulation to warm climate phases. Global Biogeochem. Cycles 32, 1605–1620. https://doi.org/10.1029/2018GB005980.

Zhang, H., Piilo, S.R., Amesbury, M.J., Charman, D.J., Gallego-Sala, A.V., Väliranta, M. M., 2018b. The role of climate change in regulating Arctic permafrost peatland hydrological and vegetation change over the last millennium. Quat. Sci. Rev. 182, 121–130. https://doi.org/10.1016/j.quascirev.2018.01.003.

Zhang, H., Väliranta, M., Piilo, S., Amesbury, M.J., Aquino López, M.A., Roland, T.P., Salminen Paatero, S., Paatero, J., Lohila, A., Tuittila, E.S., 2020. Decreased carbon accumulation feedback driven by climate-induced drying of two southern boreal bogs over recent centuries. Global Change Biol. 26, 2435–2448. https://doi.org/10.1111/gcb.15005.

Zhang, H., Väliranta, M., Swindles, G.T., Aquino-López, M.A., Mullan, D., Tan, N., Amesbury, M., Babeshko, K.V., Bao, K., Bobrov, A., Chernyshov, V., Davies, M.A., Diaconu, A., Feurdean, A., Finkelstein, S.A., Garneau, M., Guo, Z., Jones, M.C., Kay, M., Klein, E.S., Lamentowicz, M., Magnan, G., Marcisz, K., Mazei, N., Mazei, Y., Payne, R., Pelletier, N., Piilo, S.R., Pratte, S., Roland, T., Saldaev, D., Shotyk, W., Sim, T.G., Sloan, T.J., Słowiński, M., Talbot, J., Taylor, L., Tsyganov, A.N., Wetterich, S., Xing, W., Zhao, Y., 2022. Recent climate change has driven divergent hydrological shifts in high-latitude peatlands. Nat. Commun. 13, 4959. https://doi.org/10.1038/s41467-022-32711-4.

Zhang, Z., Wu, Q., Hou, M., Tai, B., An, Y., 2021. Permafrost change in Northeast China in the 1950s–2010s. Adv. Clim. Change Res. 12, 18–28. https://doi.org/10.1016/j.accre.2021.01.006.

Zhang, X., Chen, L., Ji, J., Wang, J., Wang, Y., Lan, B., 2011. Climate change and its effect in Harbin from 1881 to 2010. J. Meteorol. Environ. 27, 13–20 (in Chinese).

Zhang, Y., Liu, X., Lin, Q., Gao, C., Wang, J., Wang, G., 2014. Vegetation and climate change over the past 800 years in the monsoon margin of northeastern China reconstructed from n-alkanes from the Great Hinggan Mountain ombrotrophic peat bog. Org. Geochem. 76, 128–135. https://doi.org/10.1016/j.orggeochem.2014.07.013.